

1 Path length and sediment transport estimation from DEMs of 2 Difference: a signal processing approach

3 Lindsay Capito¹, Enrico Pandrin², Walter Bertoldi², Nicola Surian¹, Simone Bizzi¹

4 ¹Department of Geosciences, University of Padova, Padova, 35131, Italy

5 ²Department of Civil, Environmental, and Mechanical Engineering, University of Trento, Trento, 38122, Italy

6 *Correspondence to:* Lindsay Capito (lindsaymarie.capito@studenti.unipd.it)

7 **Abstract.** The difficulties of measuring bedload transport in gravel bed rivers have given rise to the morphological
8 method wherein sediment transport can be inferred from changes in riverbed elevation and estimates of the distance
9 traveled by sediment, its path length. Because current methods for estimating path length are time and labor intensive,
10 we present a method to estimate a characteristic path length from repeat digital elevation models (DEMs of difference
11 i.e., DoDs). We propose an automated method to extract the spacing between erosional and depositional sites on the
12 DoD by the application of Variational Mode Decomposition (VMD), a signal processing method, to quantify the
13 spacing as a proxy for path length. We developed this method using flume experiments where bed topography and
14 sediment flux were measured and then applied it to published field data with physical path length measured from tracer
15 measurements. Our sediment transport estimates were not significantly different than the measured sediment flux at
16 lower discharges in the lab. However, we observed an underestimation of sediment flux at the higher discharges in the
17 flume study. We interpret this as a limit of the method in confined settings, where sediment transport becomes
18 decoupled from morphological changes. We also explore how the time between survey acquisitions, the morphological
19 active width relative to the channel width, and DoD thresholding techniques affect the proposed method and the
20 potential issues they pose to the morphological method in general.

21 1 Introduction

22 In gravel bed rivers sediment transport fundamentally controls morphological processes but is notoriously difficult to
23 measure due to its spatial and temporal heterogeneity (Hoey, 1992; McLean and Church, 1999) measurement uncertainty
24 (Vericat et al., 2006), and the logistical challenges of field measurements. The morphological approach is a method to
25 estimate bedload transport based on observed changes in morphology. There have been many implementations of the
26 morphological method since its inception and it has been reviewed extensively (Ashmore and Church, 1998; Brewer and
27 Passmore, 2002; Church, 2006; Vericat et al., 2017). With the increased availability of hydrologic data and modeling
28 capabilities the morphological method has also been applied in two dimensions (x,y) by coupling a 2D hydraulic model
29 to account for sediment routing (Lane et al., 1995; Antoniazza et al., 2019; Bakker et al., 2019). These 2D applications
30 shed light on the functional links between topographic changes and spatial distribution of bedload transport. Antoniazza
31 et al., (2019) quantified the errors in estimating sediment transport with a 1D approach where 2D cross-stream sediment
32 fluxes are neglected which may be especially useful in multithreaded channels. They also explored how DEM accuracy
33 and the frequency of acquisitions affect the estimates of sediment fluxes derived by the morphological method. These
34 contributions confirm the applicability of the morphological method to estimate sediment transport, however, they require
35 intensive field campaigns and an accurate accounting of upstream water and sediment supplies, often not available in real
36 case studies. In this paper the desire is to explore novel approaches to apply the morphological method using topographic
37 data alone, as hydraulic and sediment supply data are not available in many applications and management situations.

38

39 The morphological method can be formalized based on the sediment continuity equation:

$$40 \quad (Q_{b_{in}} - Q_{b_{out}})\Delta t = (1 - p)\Delta V, \quad (1)$$

41 where $Q_{b_{in}}$ and $Q_{b_{out}}$ are the volumetric sediment flux in and out of the reach respectively, Δt is the time between
 42 surveys, p is the sediment porosity, and ΔV is the change in volume. The sediment continuity equation can be solved in
 43 several ways, but in addition to ΔV measured from the DoDs, it requires that either the incoming flux $Q_{b_{in}}$ or the
 44 outgoing flux $Q_{b_{out}}$ be defined. In most cases, neither of these fluxes are known, as they are the exact parameters that
 45 need to be estimated when applying the morphological method. This conundrum has been addressed by setting a zero-
 46 flux boundary, such as a dam or gravel sand transition (McLean and Church, 1999), by segmenting the reach such that a
 47 zero-flux boundary is set between a section of net deposition to one of net erosion (Vericat et al., 2017; Calle et al.,
 48 2020) or by measuring flux either into or out of the reach (Grams et al., 2013; Antoniazza et al., 2019).

49 Alternatively, Eq. (1) can be modified so that active layer depth, d_s , and width w_s , and the virtual velocity, v_b are used:

$$50 \quad Q_b = v_b d_s w_s (1 - p)\rho_s \quad (2)$$

51

52 Where v_b is equal to L/T , L being the distance the particles travel and T the time over which the particles are traveling
 53 (Church, 2006). The virtual velocity approach has been successfully applied using tracer gravels to estimate the path
 54 length parameter L in a variety of morphological settings (Liébault et al., 2012; Mao et al., 2017; Brenna et al., 2019,
 55 2020; Brenna and Surian, 2023). Unfortunately, tracer studies are time and labor intensive, requiring multiple site visits
 56 and intensive recovery campaigns which often have low recovery rates, especially for painted clasts (Hassan and Bradley,
 57 2017; Brenna et al., 2019). Furthermore, tracer studies are often applicable only to exposed bars, ignoring a large portion
 58 of in-channel transport, and can be sensitive to the seeding location (Liébault et al., 2012). To overcome these limitations,
 59 several methods have been proposed to estimate path length based on the connection to morphology.

60 The term path length describes the distance traveled by a particle from entrainment to deposition during a transport event
 61 and is punctuated by shorter bursts of movement termed step lengths (Einstein, 1937). Individual particles do not all
 62 entrain, travel, and deposit together in unison but rather form a distribution of path lengths potentially dependent on grain
 63 size, flow strength and duration, and channel morphology. The relative strength of these physical controls on path length
 64 has been explored with varied results. Some studies have found relationships between path length and flow metrics such
 65 as stream power (Hassan et al., 1992; Schneider et al., 2014; Vázquez-Tarrío and Batalla, 2019; Vázquez-Tarrío et al.,
 66 2019) but a considerable scatter in the data has reinvigorated the debate over the role of morphology as a primary control
 67 of path length (Hassan and Bradley, 2017; Vázquez-Tarrío and Batalla, 2019; Vázquez-Tarrío et al., 2019).

68 The connection between morphology and path length has long been discussed. Neill (1971) proposed that path length in
 69 meandering rivers should be equal to the distance from an erosional site (eroding bank) to the next depositional site (point
 70 bar) downstream. Many others have observed similar relationships based on the spacing of erosional and depositional
 71 sites and channel morphology (Beechie, 2001; Pyrce and Ashmore, 2003a, b; Hundey and Ashmore, 2009; Kasprak et
 72 al., 2015; Vázquez-Tarrío et al., 2019). Further, depositional areas (typically bars), have demonstrated a higher probability

73 of ‘trapping’ particles than erosional morphological units (McDowell and Hassan, 2020; McDowell et al., 2021). Finally,
 74 experimental research has confirmed the preferential deposition of particles specifically at bar heads and margins even in
 75 channels with more complex morphology, for example, in braided rivers (Kasprak et al., 2015) but it is reasonable to
 76 assume that in multithreaded channels, multiple path lengths might exist at different flow stages in primary and secondary
 77 channels.

78 The path length used for the virtual velocity approach is generally taken as the mean travel distance (Wilcock, 1997;
 79 Vericat et al., 2017; Mao et al., 2017; Brenna et al., 2019). However, it is unclear if the mean path length as measured by
 80 tracers is the best representation of a ‘characteristic’ path length to estimate bedload transport. To obtain an estimate of
 81 reach scale sediment transport we consider the distance travelled by the bedload involved in building geomorphic units
 82 as representative a characteristic path length. This may not necessarily be the average, as evidenced by the wide variety
 83 of path length distributions it is often the case that many or even most (the mode) of path lengths are very short, thus
 84 skewing the average depending on the distribution. For example, Pyrcce and Ashmore published synthesis of tracer studies
 85 and demonstrated that at formative discharges, particle path length distributions often exhibit primary or secondary modes
 86 corresponding to the location of bars, where deposition occurs (Pyrcce and Ashmore, 2003a). Further, flume experiments
 87 showed that the majority of particles eroded from an upstream scour pool were deposited at the point bar apex and
 88 corresponded to peaks in bi or multimodal path length distributions (Pyrcce and Ashmore, 2005). Therefore, the
 89 characteristic path length, i.e., the most representative and sound value to be used in sediment transport estimations, might
 90 be better described by these primary or secondary modes in channels with bar morphology at channel forming flows.

91 If a characteristic path length can be inferred from changes in morphology as previously discussed, advances in
 92 topographic survey techniques to acquire detailed digital elevation models (DEMs) and facilitate change detection,
 93 provide an opportunity to streamline the estimation of sediment transport. The high-resolution topography (HRT)
 94 revolution (Vericat et al., 2017) has provided an abundance of high quality surveys and an increased frequency of
 95 change detection based on the differencing of DEMs to create digital elevation models of difference (DoDs)
 96 (Brasington et al., 2000; Lane et al., 2003). Vericat et al. (2017) proposed an equation to use the path length with the
 97 volume of erosion derived directly from the DoD

$$98 \quad Q_b = (v_b \sum V_e (1 - p)\rho_s)/L_c, \quad (3)$$

99 where $\sum V_e$ is the total volume of erosion from the DoD and L_c is the length of the analyzed DEM by which the volume
 100 of erosion is normalized (Vericat et al., 2017). To use this method, L_c must be long enough for average path lengths (L)
 101 to occur and T must be short enough to prevent repeated erosion and deposition, known as compensation (Lindsay and
 102 Ashmore, 2002).

103 Redolfi (2014) attempted to estimate the path length parameter directly from the DoD using the length of individual
 104 erosional patches as a proxy for the length of the erosion-deposition sequence. This approach avoids the need to couple
 105 each erosional area to a downstream depositional area, which can be difficult to automate in multi-thread rivers. While
 106 this method scales well with flow metrics and provides reasonable estimates (Redolfi, 2014; Vericat et al., 2017), the
 107 hypothesis that the length of erosional areas is equivalent to the erosion-deposition distance has not been tested in
 108 different morphologies, and it is not clear how the survey resolution may affect the estimates by fragmenting the
 109 erosional areas into smaller parts. Recently, Calle et al. (2020) used a method of river segmentation to visualize the
 110 pattern of erosion and deposition and infer sediment connectivity as well as to estimate potential travel distances. They

111 defined boundaries between river segments and classified them into types based on their net erosional or depositional
112 characteristics. Focusing on the “type 1 depositional boundary” wherein the upstream section is erosional and the
113 immediate downstream boundary is depositional and depending on the volumes of deposition and erosion in these
114 segments they were able to estimate minimum or maximum transport distances (Calle et al., 2020). This approach
115 provides greater insight into the spatial connectivity of the river corridor and is useful to understand reach scale
116 processes. However, depending on the river, and the sections surveyed, the number of type 1 boundaries may limit the
117 applicability of the method in defining a characteristic path length and crucial information may be missed where the
118 pattern of erosion and deposition is not clear, or the periodicity spans multiple sections. For example, where there are
119 back-to-back patches of erosion or deposition or the overall pattern is separated by small areas of mixed boundaries.

120 Given the observations linking path length to morphology and building on the aforementioned methods, we seek to
121 expand on the idea that characteristic path length can be inferred from changes in morphology at near transport event
122 scale comparisons. If during a flood, sediment is mobilized from an area of erosion to an area of deposition as
123 represented on the DoD, the distance between the two should correspond to a characteristic path length. Following these
124 assumptions this work has the following objectives: i) to propose an objective and semiautomatic method to quantify a
125 characteristic path length as represented by the periodic nature of erosion and deposition from the DoD using flume
126 data; ii) to compare these estimates of a characteristic path length to measured path length distributions obtained from
127 tracer data in the field; iii) and finally to evaluate the conditions in which a characteristic path length is appropriate to
128 estimate sediment transport.

129

130 **2 Methods**

131 To meet our objectives, we use flume experiments at varying discharges with direct measurement of output sediment flux
132 and sets of repeat DEMs from which DoDs are created and used to identify patterns of erosion and deposition. We then
133 develop a semiautomated method to extract these distances between erosion and deposition as a proxy for the
134 characteristic path length and then compare our estimates of sediment flux calculated using the characteristic path length
135 to measured sediment flux. Finally, we compare the characteristic path length estimates from a published case study to
136 the physical path length distributions as measured by tracers in the field to see how the characteristic path length
137 corresponds to path length distributions.

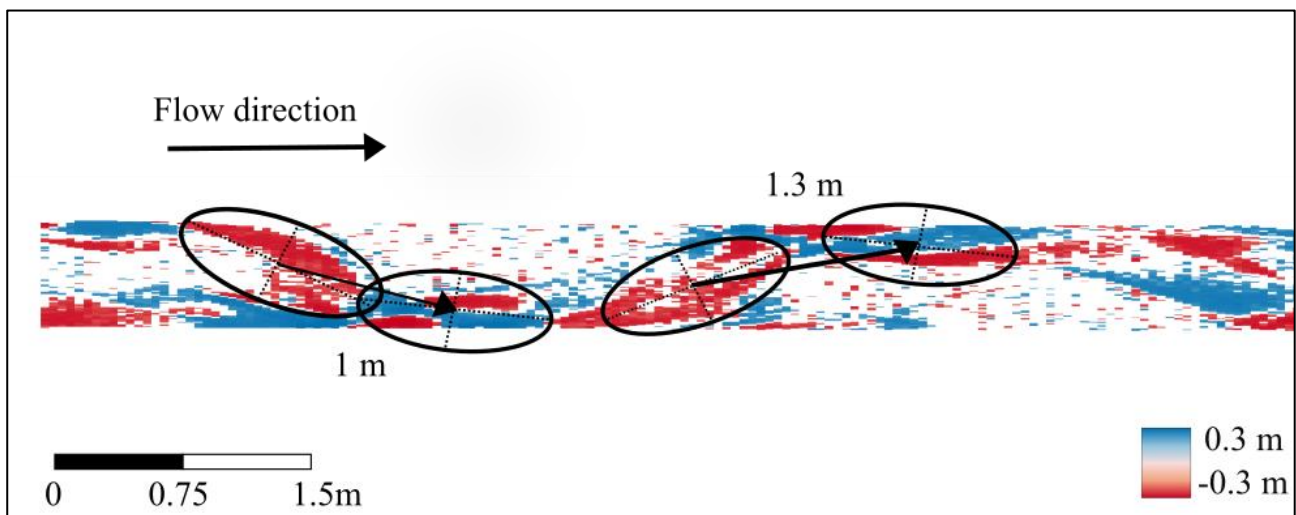
138

139 **2.1 Path length**

140

141 A key assumption inherent in our objectives is that sediment moves from an area of net erosion to an area of net
142 deposition during the time period between DEM acquisitions and that this represents a characteristic path length.
143 Ferguson and Ashworth (1992) proposed a similar method of matching specific erosional and depositional patches
144 albeit without the assistance of a DoD. This method was then implemented in the Sunwapta River, Canada (Goff and
145 Ashmore, 1994) although the authors note the difficulty in finding perfectly matching patches and conclude that
146 erosional and depositional processes are likely more dispersed. Here we will implement this “manual method” as a
147 means of comparison for the automated method presented later. The most obvious method to quantify this distance
148 between erosional and depositional sites on the DoD is to measure the spacing manually using a GIS program however,

149 this requires many subjective evaluations. Firstly, we must decide where on the patches of erosion and deposition to
 150 begin and end the measurements. Because patches of erosion and deposition are not symmetrical or of equal size, the
 151 distance between the two depends on which area of the patch we choose to begin and end the measurements. For
 152 consistency, we choose the center of the patch (Fig. 1) after Ashmore and Church (1998). Next, we must determine
 153 which patch of erosion matches with which patch of deposition which is not always obvious, and as noted previously,
 154 likely does not accurately represent the nature of bedload transport (Goff and Ashmore, 1994). Here we perform this
 155 method solely for comparative purposes and therefore used our knowledge of morphological processes to make a best
 156 estimate. For example, a patch of erosion on an outside bend likely corresponds to the deposition of the next point bar
 157 downstream (Fig. 1). Although this method is capable of producing crude estimates of path length to overcome the
 158 aforementioned biases (Ferguson and Ashworth, 1992; Goff and Ashmore, 1994; Ashmore and Church, 1998) we
 159 propose a method to estimate a characteristic path length without relying on the matching of erosion and deposition but
 160 rather to use the periodic nature of these processes. Additionally, we seek to create a method that is both objective and
 161 semiautomated.



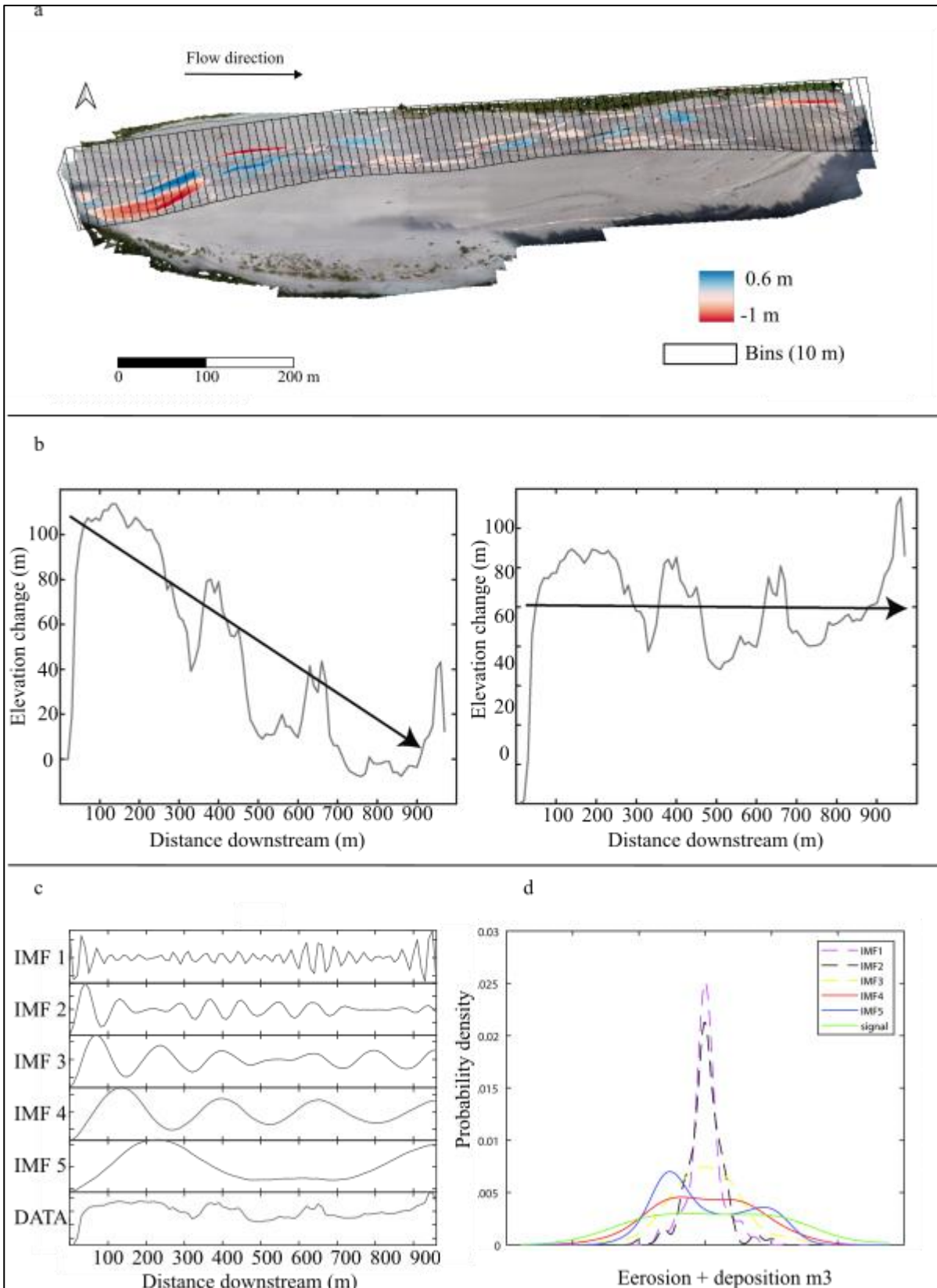
162
 163 **Figure 1: Manual method to measure spacing of erosional patches (red) and depositional patches (blue) on a**
 164 **DoD.**

165

166 2.2 Semiautomated extraction of path length

167 To visualize and then quantify the periodic nature of erosion and deposition from the DoD we simplify the spatial
 168 heterogeneity of the DoD into a vector of the net change in elevation in a streamwise direction (Fig. 2a). Because
 169 natural rivers are rarely straight, for field case studies, we must enforce a linear downstream directionality essentially
 170 straightening the bends in the river. This is achieved by segmenting the DoD into a series of equally sized “bins” using
 171 the segmentation tool of the Fluvial Corridor Toolbox (Roux et al., 2015) (Fig. 2a). The bin size can affect the pattern of
 172 erosion and deposition in that by selecting too large of bins we may miss important erosional or depositional areas when
 173 they are summed in the same bin. Similar methods that require river segmentation have proposed using the reach
 174 averaged width for the length of the bins (McDowell et al., 2021) or half of the width of the reach (McDowell and
 175 Hassan, 2020) although these studies had different objectives. Calle et al. (2020) applied a segmentation method with a
 176 similar goal of identifying corresponding zones of erosion and deposition and set the bin sized based an assessment of
 177 the river dimensions as well as the minimum transfer distance of interest. Therefore, depending on the river, the user
 178 may select differently sized bins. Once the river is segmented, we then sum the values in each bin to obtain a vector of

179 the net change in elevation in a downstream direction (Fig. 2b). In the flume studies, where there is no sinuosity, we
180 simply sum each cross section of the DoD matrix. Oftentimes a reach is aggrading or incising and therefore the net
181 vector will have an increasing or decreasing trend (Fig. 2b). Because we are interested in the spacing between areas of
182 erosion and deposition rather than the overall trend, we remove it by subtracting a best-fit linear trend from the net
183 vector (Fig. 2b). Because we simplify the heterogeneity of erosion and deposition into a net vector of elevation change,
184 we risk compensating erosion and deposition within the same cross section, therefore we also create a vector of just
185 erosion and one of just deposition as well as the net allowing for a visual comparison of the relative contribution of
186 erosion and deposition to the net as well as the periodicity of the individual processes (Fig. A1). We can see that there
187 appears to be a periodicity as the net vector oscillates forming peaks and troughs and although this periodicity seems
188 apparent, quantifying the distance is not straightforward.



189

190 **Figure 2: VMD- HD method (a) Segmentation of the DoD (example orthophoto and DoD from the Tagliamento**
 191 **River, Italy). (b) Plot of the net original and detrended vector. (c) Variational mode decomposition (VMD) with 5**
 192 **intrinsic mode functions (IMFs). (d) Probability density function (PDF) of each IMF and the original net vector.**

193 One approach could be to count the zero crossings and then use that distance as the proxy for path length. However, we
 194 risk measuring low magnitude spikes that cross zero that may not necessarily represent the overall periodicity or large

195 oscillations that don't cross the zero line. A smoothing filter may be used to remove these low magnitude oscillations
196 but we risk losing potentially relevant information. To solve this problem, we turn to the realm of signal processing
197 where the practice of "denoising" and extracting information from oscillations is ubiquitous.

198 Signal processing is a field that deals regularly with extracting information and patterns that are not visually apparent
199 and its applications have been used in a wide variety of settings including voice recognition (Sigmund, 2003; Upadhyay
200 and Pachori, 2015), medical applications (Boudraa et al., 2005; Liu et al., 2008), and even time series analysis of
201 climate data (Barnhart and Eichinger, 2011). There are many approaches to de-noising including Fast Fourier transform,
202 empirical mode decomposition (EMD), and wavelet analysis. Each of these methods come with inherent strengths and
203 weaknesses, for example wavelet analysis requires that a mother wavelet be selected a priori and may influence the
204 results (Boudraa et al., 2005). We chose to use variational mode decomposition (VMD) due to its robustness with
205 respect to sampling and noise and the ability to handle signals that exhibit non-linearity and non-stationarity
206 (Dragomiretskiy and Zosso, 2014; Huang et al., 2016; Ma et al., 2017). VMD decomposes the signal into a set of
207 intrinsic mode functions (IMFs) each with a different central frequency (Dragomiretskiy and Zosso, 2014; Ma et al.,
208 2017) (Fig. 2c). In this case of our static 'signal' the frequency is more accurately described as the wavelength. It is
209 beyond the scope of this paper to describe the mathematics of VMD in detail, therefore, for a complete explanation see
210 (Dragomiretskiy and Zosso, 2014; Huang et al., 2016; Ma et al., 2017; Upadhyay and Pachori, 2015).

211 Once the original net vector of erosion and deposition is decomposed into the various IMFs, we need to select the IMF
212 or IMFs that most accurately represent the periodicity of the original data and therefore our characteristic path length.
213 Ma et al. (2017) proposed a method to select the most relevant IMF, and therefore periodicity of the signal, by
214 computing the probability density function (PDF) using kernel density smoothing for each of the five IMFs and of the
215 original data vector (Fig. 2d), then to calculate the Hausdorff distance (HD), a metric of geometric similarity, between
216 each IMF's PDF and the PDF of the original data and select the IMF most geometrically similar to the original data (Ma
217 et al., 2017) (hereafter VMD-HD method). In most cases, the longer wavelength IMFs most closely resemble the
218 original signal whereas the IMFs with shorter wavelengths are more likely associated with noise (Boudraa et al., 2005).
219 The computed wavelength is converted to a meaningful physical quantity by multiplying by the bin spacing in meters.
220 Because we are interested in the distance from peak to trough, we divide the period by two to obtain the path length
221 proxy (Neill, 1971; Ashmore and Church, 1998). Although this method allows for the selection of one IMF to
222 presumably represent the periodicity of the data, we record path lengths calculated from the other IMFs to evaluate the
223 range of estimates generated by the decomposition and determine if the VMD-HD method is appropriate for
224 determining a characteristic path length and the relative importance of other IMFs. All calculations were performed in
225 MatLabR2020b using the built in VMD function and the Hausdorff distance function (Danziger, 2023).

226 One important consideration when using VMD to decompose a signal is that is the user must define the number of IMFs
227 beforehand. The number of IMFs is important as under binning, choosing too few IMFs, may mean that critical IMFs
228 are missed, whereas over binning, can cause duplication of components (Wu et al., 2020). In signal processing, there are
229 sophisticated methods for determining the number of IMFs, for a summary see (Wu et al., 2020). However, for our
230 purposes and simplicity's sake, we performed a brief sensitivity analysis based on the property of convergence often
231 used in the signal processing methods (Wu et al., 2020; Huang et al., 2016; Ma et al., 2017). The default setting in the
232 MatLab function is 5 IMFs, we used 3, 5, 8, 15, and 25 IMFs to calculate path length and assessed how it changed for
233 the maximum IMF (Fig. A2). We found that using more IMFs generally increased the number of high frequency
234 components rather than the lower frequency IMFs (Fig. A3). Because these higher frequencies are generally associated

235 with noise and in our case are physically too small to likely represent meaningful path lengths (on the order of
 236 millimeters) we decided more than 5 IMFs did not contribute physically meaningful information in that the IMFs with
 237 longer wavelengths did not change drastically. We also determined that 3 IMFs were too few as it was clear that the
 238 longer wavelengths were missing (Fig. A3). Therefore, we chose to use the default 5 IMFs as this provided a
 239 manageable number of components while effectively separating the lower frequencies. This is a convenient starting
 240 point for assessing the VMD method as a tool to extract the periodicity as a proxy for characteristic path length but is by
 241 no means the only option. We encourage further exploration of the IMF parameter in future applications and as the
 242 method is refined.

243 3 Flume and field data

244 The method was tested using data from a set of flume runs performed in the Hydraulic Laboratory of the University of
 245 Trento, where DEMs were generated for fixed time intervals and varying discharges, and direct measurements of the
 246 bedload flux were also collected. To test the efficacy of the method in the field, we selected a published dataset of
 247 measured path lengths with corresponding DoDs for the San Juan River in British Columbia Canada (McQueen et al.,
 248 2021). Although McQueen et al. deployed tracers in four separate periods, there was only one deployment (2018-2019)
 249 with corresponding DEMs (McQueen et al., 2021). DoDs and corresponding tracer data were available for three
 250 separate sites (bar 6, bar 7, and bar 15) for the 2018-2019 period. Detailed information on their collection and
 251 processing can be found in McQueen et al., 2021.

252 3.1 Flume experiments

253 The Trento laboratory experiments were carried out in a 0.6 m wide and 24 m long flume, filled with nearly uniform 1
 254 mm diameter sand. The flume slope was set to 0.01 m/m. Topographic surveys were performed over the final 14 m of
 255 the flume, to limit the upstream inflow effects, using a laser gauge, mounted on a movable deck. The longitudinal and
 256 crosswise spacings were 0.05 m and 0.005 m, respectively. Four sets of nine runs were performed, with the flow
 257 discharge set to 0.7, 1, 1.5, and 2 l/s, which correspond to a range of different planform morphologies (Table 1).
 258 Sediment input at the upstream end of the flume was constant in each run, with a flux equal to the average measured at
 259 the downstream end, as computed in a preliminary set of experiments. Therefore, the overall average bed elevation of
 260 the runs was in equilibrium, with no net erosion or deposition. The runs were performed following the same procedure,
 261 involving three phases of different lengths, based on the transport condition of each discharge. These durations were
 262 estimated referring to the time scale for morphological evolution computed from the sediment balance mass equation
 263 (Garcia Lugo et al., 2015), which can be expressed as:

$$264 \quad T_{ex} = \frac{DW^2}{Q_b}, \quad (4)$$

265 where D is the average flow depth and W is the flow width. Table 1 provides the values of T_{ex} for each flume
 266 experiment.

267 **Table 1: Initial conditions for each dataset including the type of validation data.**

	Flume 1	Flume 2	Flume 3	Flume 4	San Juan Bar 6	San Juan Bar 7	San Juan Bar 15
Peak discharge (m ³ /s)	0.0007	0.001	0.0015	0.002	942	942	942
Slope (m/m)	0.01	0.01	0.01	0.01	0.0038	0.0031	0.0009
Width (m)	0.6	0.6	0.6	0.6	150	150	130

D_{50} (m)	0.001	0.001	0.001	0.001	0.05	0.056	0.042
Time scale T_{ex} (min) (eq.4)	94	50	38	30	-	-	-
Time between surveys (min)	47	25	19	15	~1 year	~1 year	~1 year
ω * Dimensionless stream power	0.15	0.22	0.33	0.43	0.76	0.61	0.31
Validation Data	Sediment Flux	Sediment Flux	Sediment Flux	Sediment Flux	RFID tracers	RFID tracers	RFID tracers
Planform	Wandering	Wandering	Wandering transitional	Alternate bar	Wandering	Wandering	Wandering

268

269 First, an initial phase of about 12 times this time scale T_{ex} with constant flow was run, to ensure the formation of a
 270 near-equilibrium morphological condition, starting from a flat sand bed scraped to the prescribed slope. This was
 271 followed by a long run, at constant discharge, lasting 19 times the time scale T_{ex} , aimed at measuring the output
 272 sediment flux. This was continuously monitored at the channel outlet, through a permeable basket placed on four load
 273 cells. Sediment flux was measured every minute. After a bed topography survey, the third phase was a sequence of nine
 274 shorter runs, lasting 0.5 times the time scale T_{ex} , each followed by a bed topography survey, which produced nine
 275 corresponding DoDs. The duration of these nine runs (and therefore the time interval between surveys) was decided to
 276 have easily measurable changes of the bed morphology, without having significant compensation processes.

277 The DoDs were created by subtracting two consecutive DEMs, then underwent a three-step filtering process to highlight
 278 the relevant erosion and deposition patterns, removing most of the noise associated with the surface roughness and
 279 measurement accuracy. First, the DoDs were filtered considering a uniform detection threshold equal to 2 mm (2 times
 280 the D_{50}), meaning that erosion or deposition values lower than this threshold are set to zero. Thereafter, a spatial average
 281 was performed as a moving average on three values along the transversal direction where the DoD discretization is the
 282 finest. Lastly, a despeckling algorithm removed all isolated cells, both considering single cells that show erosion or
 283 deposition, as well as single cells that show no change. This last step was implemented to keep the detection threshold
 284 as low as possible while removing unphysically small areas. Additionally, we calculated the morphological active width
 285 by determining the percentage of the DoD that showed morphological activity (i.e., was not zero after filtering).

286 3.2 San Juan River data

287 To compare the characteristic path length to measured path length distributions in the field, we used data from the San
 288 Juan River, located on Vancouver Island, British Columbia with a drainage area of approximately 730 km² and a mainly
 289 rainfall driven hydrology (McQueen et al., 2021). The reach of interest in this study was alluvial in nature with a
 290 wandering morphology and a substrate composed of gravel, cobble, and sand (McQueen et al., 2021). The time in
 291 between acquisitions is one year, in which it is estimated there were five flood events able to generate sediment
 292 transport using a threshold of 500 m³ s⁻¹, which was visually estimated by the authors to be equivalent to the bankfull
 293 discharge (McQueen et al., 2021). DEMs were generated by LiDAR acquisitions and have a spatial resolution of 10 cm
 294 and a vertical root mean square error lower than 10 cm. Topographic changes between survey dates were then
 295 calculated by processing the LiDAR DEMs using the Geomorphic Change Detection (GCD) software (Wheaton et al.,
 296 2010). More information on how they were obtained and processed including the spatially variable thresholding
 297 techniques can be found in McQueen et al. (2021). The LiDAR-derived DoDs were used to interpret patterns of tracer
 298 displacement and burial depths and to provide information on the morphological development of the bars during the
 299 study period. However, they do not provide complete reach-scale sediment budgets due to the lack of in-channel

300 topographic data and stage differences during each LiDAR survey affecting the relative portion of the river bed that was
 301 exposed. Nevertheless, we believe the exposed part of the channel, the bars, and associated patches of erosion and
 302 deposition (see Fig. 9b) are sufficient to be used with our proposed method to estimate path lengths and be compared
 303 with field measured path lengths from the tracer data. This is because we are not calculating sediment flux for the San
 304 Juan River and are only interested in comparing our estimates of the characteristic path length to the measured tracer
 305 distributions. As far as the pattern of erosion and deposition and how that may be disrupted, we believe that because the
 306 submerged area is small relative to the DoD the pattern should not change drastically. Further, by looking at figures 15
 307 and 16 from McQueen et al. (2021) we can see that the tracers were largely recovered from the exposed bar surfaces in
 308 the 2018-2019 deployment. This gives us confidence that the deposition we are measuring corresponds largely to the
 309 deposition associated with the tracers. Although this is not an ideal situation, we believe the benefits outweigh the
 310 limitations considering the difficulty of finding high quality RFID tracer data and corresponding DoDs. The San Juan
 311 River DoDs were downloaded directly from the Scholars Portal Dataverse (<https://doi.org/10.5683/SP2/UQGZCG>). The
 312 DoDs were segmented using similar principles to Calle et al. (2020) in a similarly sized river, therefore the bin size was
 313 conservatively set at 10 m.

314 3.3 Validation and error estimation

315
 316 Each study had unique initial conditions including slope, discharge, grain size, channel configurations, and time/flood
 317 events between surveys (Table 1). Because the studies vary with respect to these initial conditions, we calculated the
 318 dimensionless stream power (ω^*) after Bertoldi et al. (2009) to compare them as:

$$319 \quad \omega^* = \frac{Q \cdot S}{W \sqrt{g \Delta D_{50}^3}}, \quad (5)$$

320 where Q is the peak discharge, S is slope, W is the average wetted width, Δ is the relative submerged density, D_{50} is the
 321 median grain size, and g is the acceleration due to gravity.

322 For the flumes, we used estimates of path length generated by the VMD-HD method and those associated with the two
 323 longest wavelengths, IMF 4 and IMF 5 separately to calculate the virtual velocity Eq. (2) and sediment flux Eq. (3)
 324 which we then compared to measured flux data. The measured sediment flux during the initial long run showed high
 325 variability, with phases of high and low sediment flux lasting several tens of minutes. For this reason, we prefer to use
 326 the data from the long runs, from which we estimated an average sediment flux of 0.33 g/s (SD=0.17) for the 0.7 l/s
 327 discharge, 0.78 g/s (SD=0.31) for the 1 l/s discharge, 1.98 g/s (SD=0.65) for the 1.5 l/s discharge, and 3.22 g/s
 328 (SD=0.79) for the 2 l/s discharge. We subdivided the second phase into 38 intervals of 0.5 T_{ex} duration, equal to the
 329 duration as the short runs in phase 3, and computed the variability of the flux over this range.

330 We used ANOVA to compare path length, virtual velocity, and erosion across the four discharges ($\alpha=0.05$) and a Post-
 331 hoc Tukey test to explore significant differences between discharges. To compare the measured sediment flux to the
 332 estimates from the VMD-HD method and the IMF 4 and IMF 5 estimates we used a student's t-test ($\alpha=0.05$). And
 333 finally, to compare the error of our path length and sediment transport estimates we calculated the relative percent error
 334 δ in order to compare the sediment flux estimates to that of the long runs of average sediment flux as:

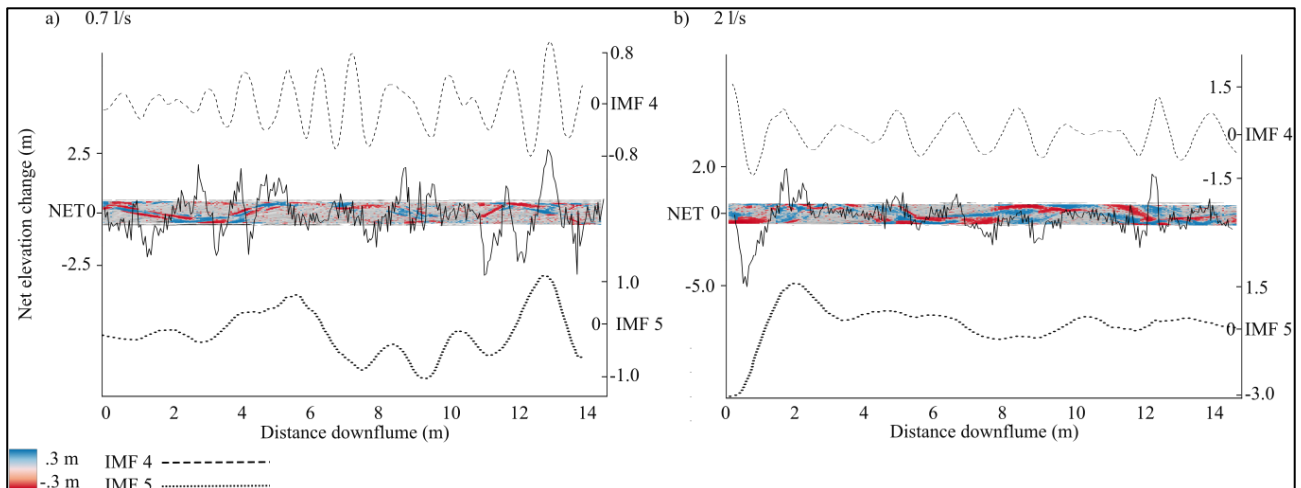
$$335 \quad \delta = \frac{|E-M|}{M}, \quad (6)$$

336 where E is the average of the estimated sediment flux for the 9 runs at a given discharge and M is the averaged
 337 measured sediment flux from the long run at the same given discharge. For the San Juan River we compared the VMD-
 338 HD estimates of path length and IMFs 4 and 5 qualitatively to the published path length distributions and the locations
 339 of mean, median, and modes. The tracer recovery locations were accessed in spreadsheet form and in keeping with the
 340 analysis of the authors we disregarded any tracers that moved less than 10 m before calculating the path length
 341 distributions.

342 4 Results

343 4.1 Flume experiment

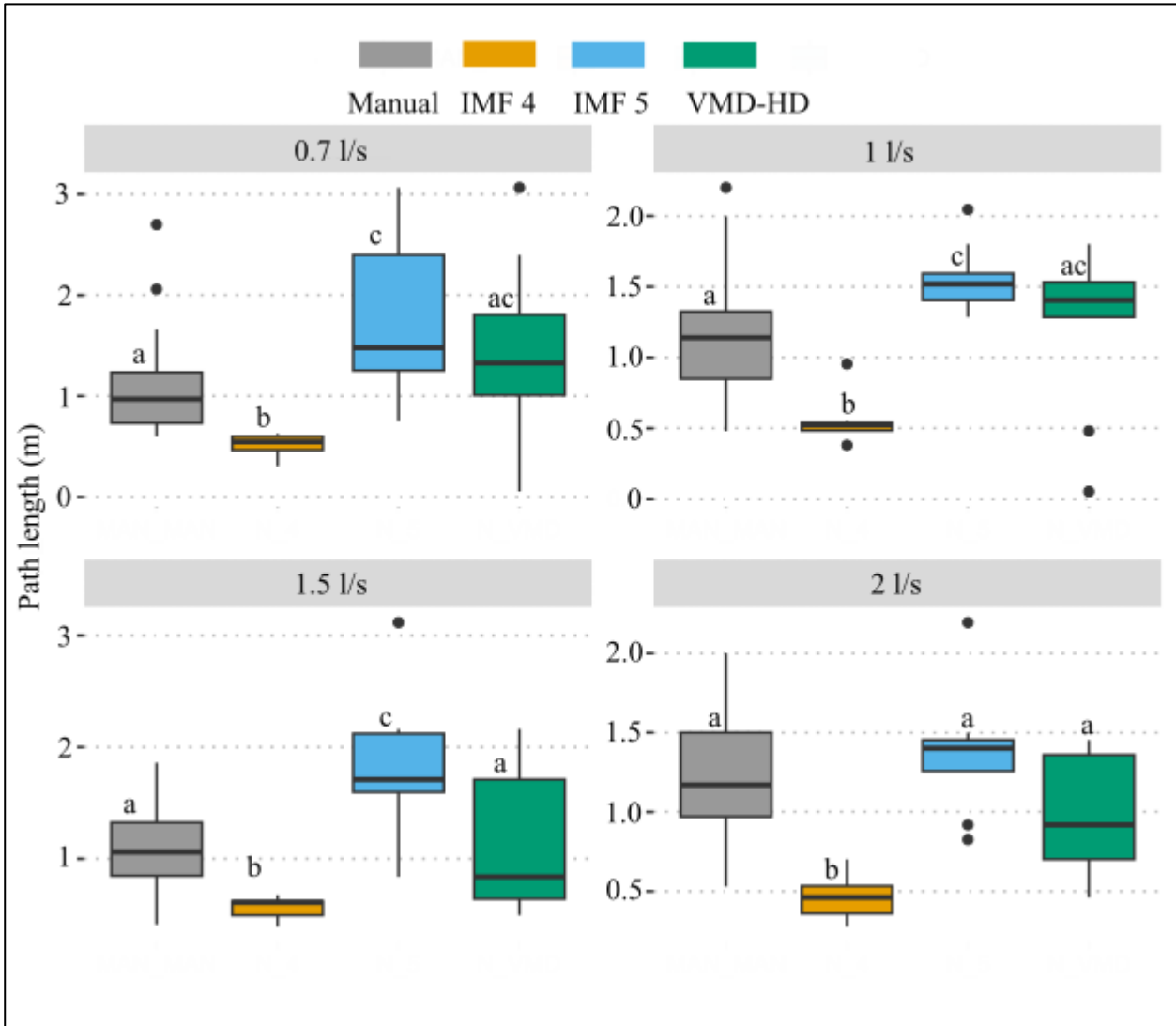
344 To aid in the interpretation of the results, Fig. 3 shows a DoD from the lowest discharge, 0.7 l/s (a) and the highest
 345 discharge, 2 l/s (b) with the net vector (continuous line), IMF 4 (dashed line), and IMF 5 (dotted line) as obtained from
 346 the VMD method. Oftentimes the areas of deposition and erosion from the DoD correspond clearly to the IMF 4 and 5
 347 vectors as with the 0.7 l/s discharge where areas of deposition are concave and areas of net erosion correspond to
 348 convex areas of the vector (Fig. 3a). At the higher discharges (1.5 l/s and 2 l/s) the total area of morphological activity
 349 increases and patches of erosion and deposition begin to overlap, creating a more chaotic and difficult to discern pattern
 350 (Fig. 3b, A1). We also observed a similar periodicity in the erosional and depositional vectors and at the 2 l/s discharge
 351 the depositional vector appears to show this most clearly (Fig. A1).



352
 353 **Figure 3: DoDs from 0.7 l/s discharge (a) and 2 l/s discharge (b) with the net vector of elevation change laid over**
 354 **the top. IMF 4 vector (above, dashed line) and IMF 5 vector (below, dotted line)**

355 In the flume experiment, the VMD-HD method of choosing the most relevant IMF selected the longest wavelength IMF
 356 5 71% of the time and IMF 4 23% of the time. IMFs 2 and 3 were never selected and IMF 1 was selected only twice.
 357 However, at the higher discharges (1.5 l/s and 2 l/s) IMF 4 was selected more frequently, thereby reducing the average
 358 path length when compared to the lower discharges (Fig. A4). Using the selected IMFs, the VMD-HD method
 359 estimated a similar average path length for all of the discharges (Fig. 4). The averages were, 1.45 m (standard deviation
 360 (SD) = 0.93) for the 0.7 l/s discharge runs, 1.24 m (SD=0.58) for the 1 l/s runs, 1.21 m (SD = 0.58) for the 1.5 l/s runs,
 361 and 1 m (SD = 0.37) for the 2 l/s runs (Fig. 4). The path length estimates derived from IMF 4 were similar for all
 362 discharges, 0.51 m (SD=0.12) for the 0.7 l/s discharge, 0.55 m (SD=0.16) for the 1 l/s discharge, 0.56 m (SD=0.91) at
 363 the 1.5 l/s discharge, and 0.46 m (SD=0.15) at 2 l/s (Fig.4) with no significant differences between the discharges ($p >$
 364 0.05). The path lengths derived from IMF 5 were also similar between the discharges with no significant differences ($p >$
 365 0.05) and were, 1.75 m (SD=0.79) for the 0.7 l/s discharge, 1.55 m (SD=0.24) for the 1 l/s discharge, 1.79 m

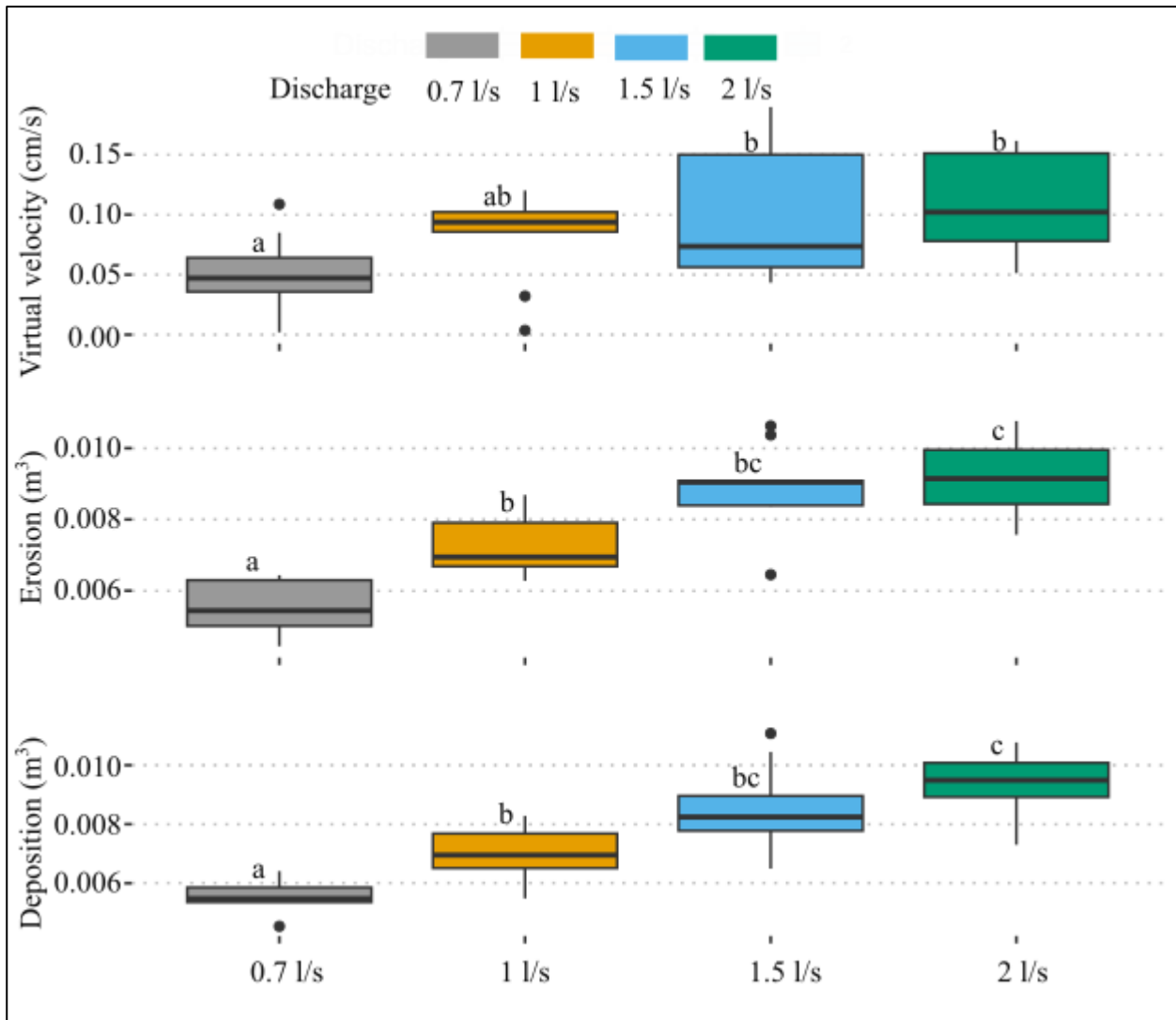
366 (SD=0.67) for the 1.5 l/s discharge, and 1.37 m (SD=0.39) for the 2 l/s discharge (Fig. 4). The VMD-HD method
 367 matched closely with the manually measured distances and there were no statistically significant differences for any of
 368 the discharges (p-value > 0.05) (Fig. 4) while the IMF 4 and IMF 5 derived path lengths bracket the manually measured
 369 distances and the VMD-HD selected path lengths (Fig. 4).



370

371 **Figure 4: Path length estimates from the manual method (gray), IMF 4 (orange), IMF 5 (blue), and the VMD-HD**
 372 **method (green). Significant differences from the post-hoc Tukey test are denoted by letters a-c.**

373 The estimated path lengths were not significantly different between the discharges (p-value >0.05) and showed no
 374 obvious trend of increasing or decreasing with discharge. However, when used to calculate the virtual velocity (v_b)
 375 wherein the path length is divided by the time between surveys (Table 1), we see an increase in the virtual velocity with
 376 discharge (p-value < 0.05) (Fig. 5). Likewise, the average volumes of erosion and deposition calculated from the filtered
 377 DoDs increases significantly with discharge (p-value < 0.001) (Fig. 5).



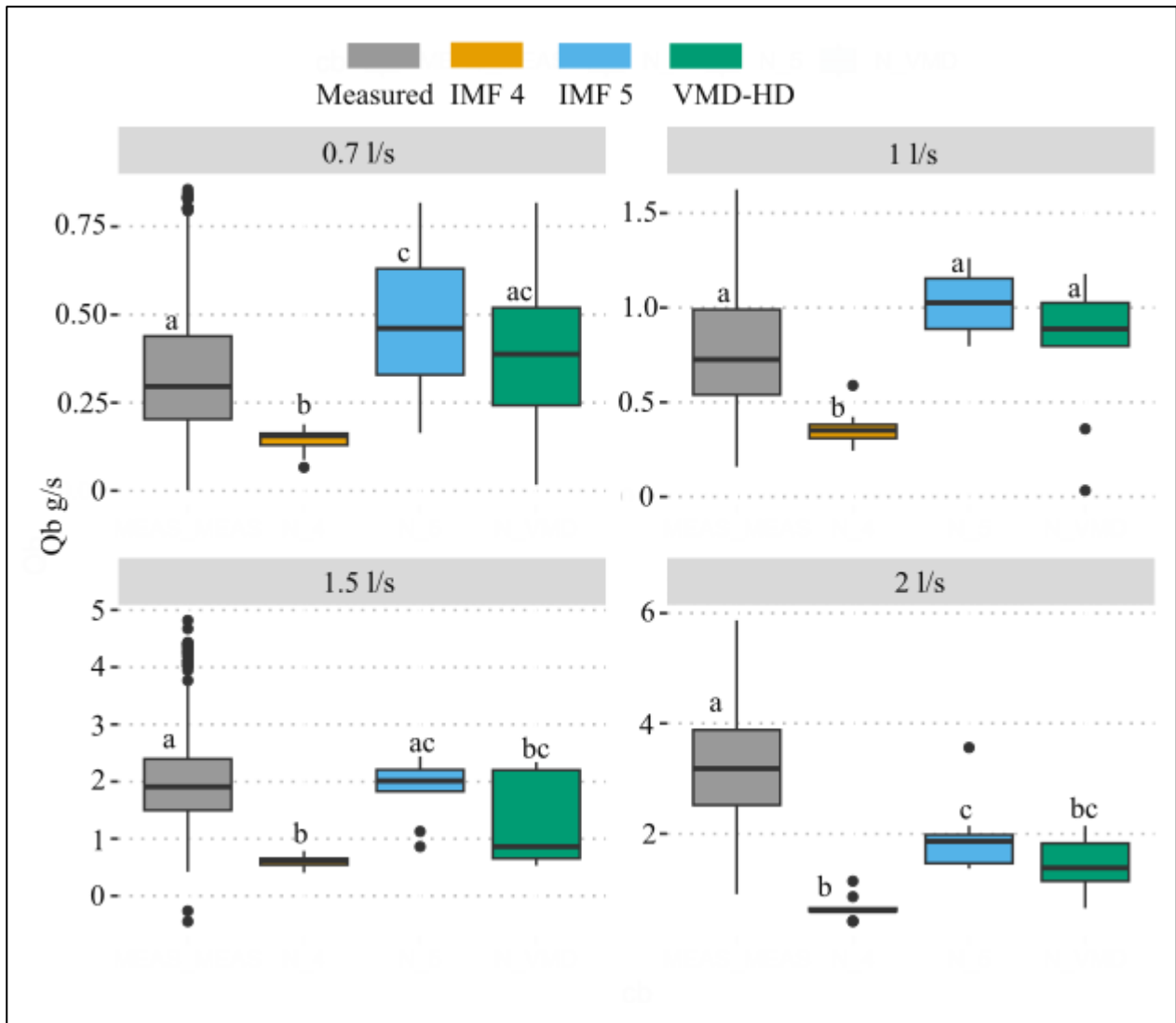
378

379 **Figure 5: Estimated virtual velocity using the VMD-HD path length estimates, measured volumes of erosion and**
 380 **deposition for each discharge. Significant differences from the Post hoc Tukey test are denoted by letters a-c.**

381 When used to calculate sediment transport Eq. (3) the VMD-HD method corresponds well to the measured average for
 382 the lower discharges (0.7 l/s and 1 l/s) whereas at the higher discharges (1.5 l/s and 2 l/s) the method significantly
 383 underestimated the measured flux (Fig. 6). For the 0.7 l/s discharge, the VMD-HD method estimated a rate of 0.39 g/s
 384 (SD = 0.25) averaged over the nine runs, which was not significantly different than the measured average of 0.33 g/s
 385 (SD = 0.18) and the relative percent error (δ) was 18%. For the 1 l/s discharge the method estimated 0.81 g/s (SD =
 386 0.38) and was not significantly different than the measured average of 0.78 g/s (SD= 0.30, δ = 4%). At the higher
 387 discharge of 1.5 l/s the average estimated by the VMD-HD method was 1.33 g/s (SD = 0.82) whereas the measured
 388 average was 1.98 g/s (SD = 0.70) (p-value < 0.05, δ =32%). Finally, for the 2 l/s runs the estimated average was 1.41g/s
 389 (SD = 0.48) whereas the measured average was 3.22 g/s (SD = 0.98) (p-value < 0.001, δ = 56%) (Fig. 6).

390 If we use just the IMF with the longest wavelength (IMF 5) to estimate path length and calculate sediment transport, we
 391 slightly overestimate sediment transport at the 0.7 l/s discharge, 0.48 g/s although not significantly ($p > 0.05$, δ = 45%)
 392 (Fig. 6). At the 1 l/s discharge IMF 5 significantly overestimates the average flux with an estimate of 1.03 g/s ($p < 0.01$,
 393 δ = 32%). At the 1.5 l/s discharge the estimated flux of 1.88 g/s using the IMF 5 path lengths was not significantly

394 different from the measured flux ($p > 0.05$, $\delta = 5\%$) (Fig. 6). However, using the IMF 5 path lengths still significantly
 395 underestimated sediment flux at the 2 l/s discharge, 1.95 g/s ($p < 0.001$, $\delta = 39\%$) (Fig. 6).



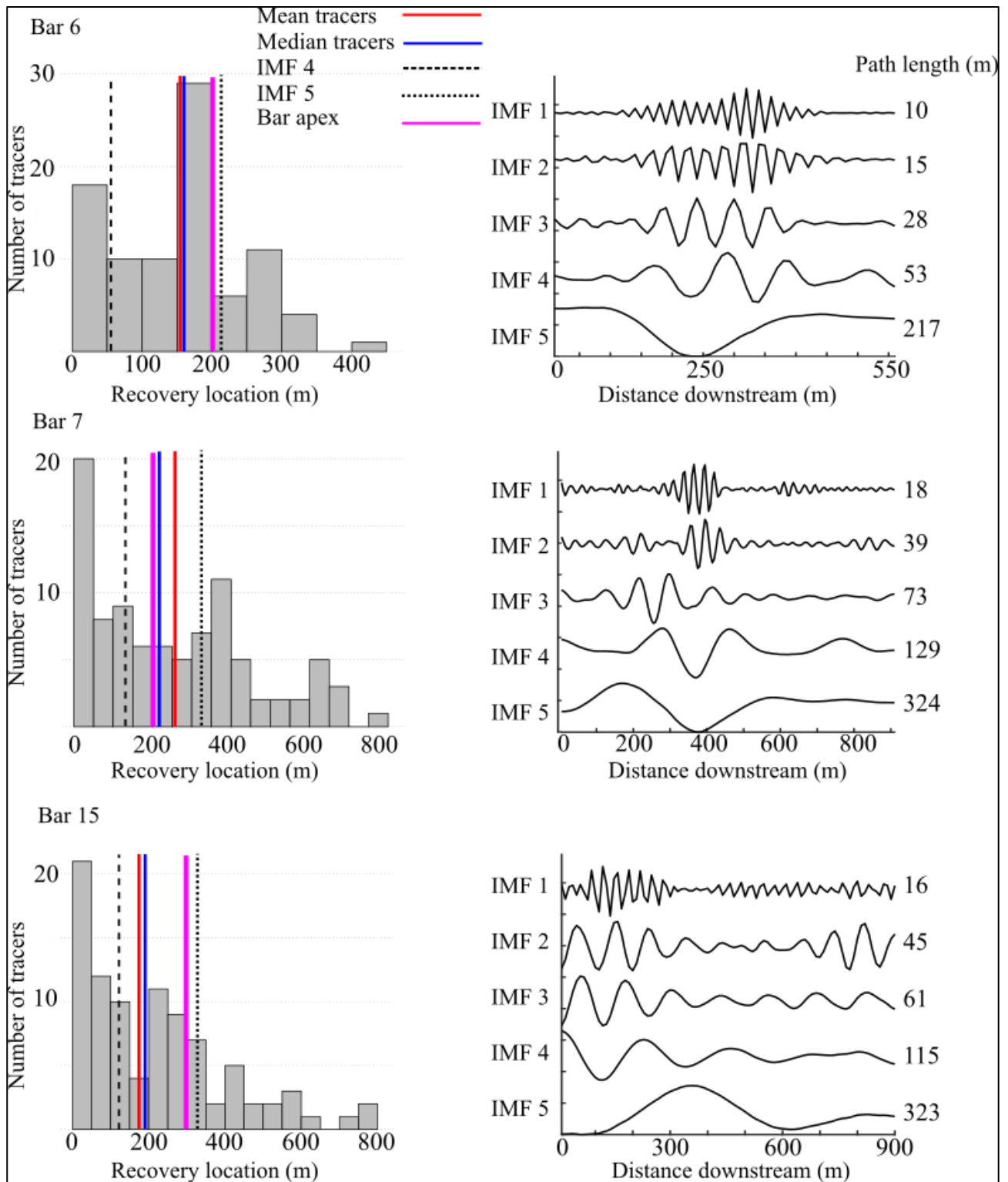
396
 397 **Figure 6: Measured sediment flux (gray) compared to the estimates calculated using IMF 4 (orange), IMF 5**
 398 **(blue), and the VMD-HD method (green). Significant differences from the post-hoc Tukey test are denoted by**
 399 **letters a-c.**

400 Using the second longest wavelength, IMF 4, we underestimate at all of the discharges (Fig. 6). The estimated flux was
 401 0.14 g/s at the 0.7 l/s discharge ($\delta = 58\%$), 0.36 g/s at the 1 l/s discharge ($\delta = 54\%$), 0.61 g/s at the 1.5 l/s discharge
 402 ($\delta = 69\%$), and 0.65 g/s at the 2 l/s discharge ($\delta = 80\%$), (all p values < 0.001) (Fig. 6).

403 4.2 San Juan River

404 The 2018-2019 year for which we conducted our analyses, was moderate in terms of excess flow energy with 5 flood
 405 events exceeding a discharge of $500 \text{ m}^3 \text{ s}^{-1}$ and a peak discharge of $942 \text{ m}^3 \text{ s}^{-1}$. The path length distributions of bar 7
 406 and bar 15 are positively skewed although there is a secondary mode in the bar 7 distribution corresponding roughly to
 407 the bar tail (Fig. 7) whereas the distribution of bar 6 is bi-modal with the primary mode corresponding to the bar apex
 408 (Fig.7). This is potentially because bar 6 had the most pronounced curvature, perhaps contributing to the clustering of
 409 deposition just before the apex, where a migrating gravel sheet terminated (McQueen et al., 2021). This bar apex
 410 corresponds with the path length from IMF 5 of 217 m which was selected from the VMD-HD method (Fig. 7). IMF 5

411 was also selected by the VMD-HD method for bar 7 equaling 324 m, and here we see a correspondence to the small
412 secondary mode where the authors note there was a clustering of tracers (Fig. 7) (McQueen et al., 2021). Again, IMF 5
413 with a path length of 323 m was also selected for bar 15 and corresponds closely to the bar apex, although there was not
414 a clustering of tracer deposition in this deployment as observed in the year with higher discharge (Fig. 7). Additionally,
415 bar 15 had the highest proportion of sand which is not represented by the tracers, potentially contributing to the
416 discrepancy between our estimates and the tracers. IMF 4 was always well below the lengths associated with the bar
417 apexes, and the median and mean tracer distances (Fig. 7). However, the bar apexes and the median and mean tracer
418 distances were always between IMF 4 and IMF 5 (Fig. 7). The range between IMF 4 and IMF 5 accounted for 62% of
419 the path length distribution for bar 6, 36% for bar 7, and 45% for bar 15.



420

421 **Figure 7: Tracers-based path length distributions (on the left) and VMD derived IMFs for bars 6,7, and 15 from**
 422 **the San Juan River dataset. IMF 4 (dashed line), IMF 5 (dotted line), mean tracer distance (red), median tracer**
 423 **distance (blue), and the bar apex (pink) are shown over the path length distributions.**

424 5 Discussion

425 We developed a method to estimate the characteristic path length during a given flood using information inherent to the
 426 DoD by applying the principle that at channel-forming flows, the majority of particles move from an area of erosion to
 427 the next area of deposition downstream (Pyrce and Ashmore, 2003a, b). By using the periodic nature of erosion and

428 deposition we overcome the subjectivity and time involved in measuring these distances manually while aligning
429 closely with these manually measured distances (Fig. 4). When evaluating the efficacy of our proposed method it is
430 important to keep in mind the uncertainty of even direct measurement of sediment transport. The spatial and temporal
431 frequency required to overcome the noise of measurement uncertainty (i.e., achieve an acceptable signal to noise ratio)
432 in some cases can require sub-daily monitoring with precise equipment (Grams et al., 2019). The variability of sediment
433 transport measurements in the flume study ranged from a standard deviation of approximately 30% to over 50% of the
434 averaged flux (Fig. 6). Given this high variability, our reach scale averages were not significantly different from the
435 measured averages for the 0.7 l/s and 1 l/s discharges (Fig. 6). Importantly, we observed that the method underestimates
436 the sediment flux significantly for the two highest discharges in the lab where the bed shows a higher percentage of the
437 width experiencing topographic change (Fig. 6). The method presented to estimate a characteristic path length using
438 only remotely sensed data shows promising results under certain conditions and provides insight into conditions where
439 it is not applicable.

440 **5.1 Path length estimation by VMD-HD method: limitations and perspectives**

441 **5.1.1 Flow effects**

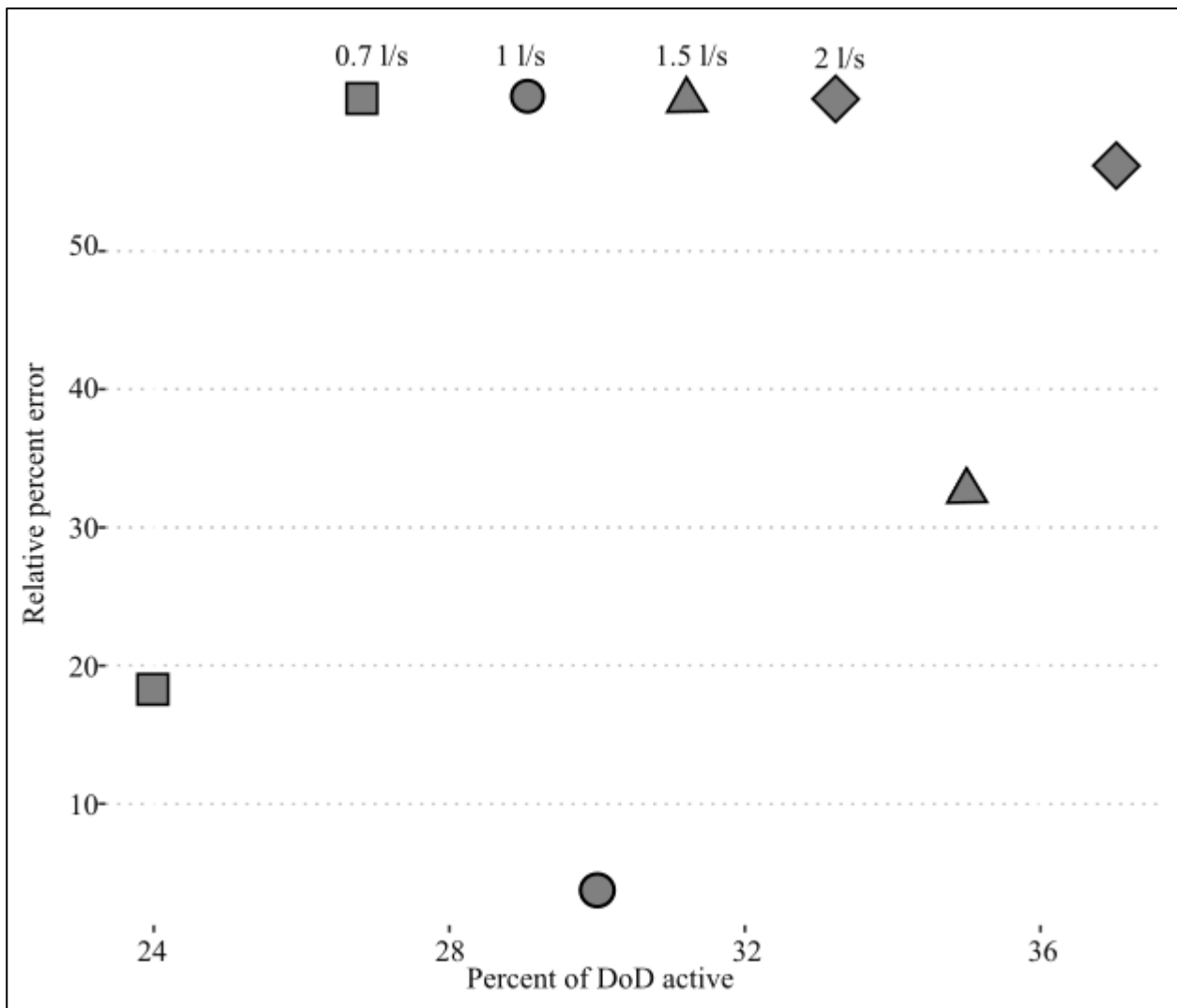
442 Previous studies have shown a relationship between path length and hydrologic variables such as discharge, stream
443 power, and excess shear stress (Hassan et al., 1991; Pyrcce and Ashmore, 2003b). A notable result of the flume
444 experiment is that the estimated path length did not significantly differ between the four discharges (Fig. 5). We
445 propose two possible explanations for this discrepancy with the literature. First, it is possible that the actual path length
446 is increasing with discharge as has been observed in previous studies (Hassan et al., 1991; Pyrcce and Ashmore, 2003b)
447 but the method fails to capture it because the VMD-HD method is based on the spacing of erosion and deposition which
448 does not change for the varying discharges under the flume conditions. It is possible that at higher discharges the
449 characteristic path length, that we define as the distance from net erosional areas to net depositional areas, is not
450 appropriate under the higher flow conditions because most particles are moving farther than the next depositional site
451 downstream. This violates the assumption on which our method is based and is impossible to prove in our experiment
452 without tracers. We can however look to literature to understand the conditions in which tracers tend to travel more than
453 one morphological unit (Liébault et al., 2012; Vázquez-Tarrío et al., 2019) and coupled with future studies, perhaps
454 determine the conditions under which a characteristic path length is inappropriate to estimate sediment transport.

455 From the San Juan River data we see that for a year with moderate flow, as characterized by the authors, that very few
456 tracers traveled further than the first depositional site downstream of their insertion point (McQueen et al., 2021).
457 However, the moderate flow year for which we had corresponding tracer and DoD data resulted in two of the three sites
458 with positively skewed distributions, and only bar six showing a mode near the bar apex, which also corresponded to
459 the IMF 5 path length (Fig. 7). The moderate flow conditions could explain why our estimates lined up more closely
460 with the bar apex for bar 15, where in the previous high flow year the majority of tracers were deposited resulting in a
461 symmetrical distribution (Fig. 8 from McQueen et al., 2021). It could be that our method is strongly influenced by the
462 morphology of the channel such that when flow is insufficient to create symmetrical or bi modal path length
463 distributions, we overestimate by using the characteristic path length because the majority of particles are not reaching
464 the next major depositional site downstream (i.e., a positively skewed distribution). Additionally, when the flow
465 exceeds a yet unidentified threshold, the majority of particles move more than one depositional site downstream and
466 therefore we underestimate sediment transport by using the characteristic path length. We can speculate that this is
467 happening to some extent in the flume experiment. We see that at the lowest discharge, 0.7 l/s, we slightly overestimate

468 the sediment flux especially using IMF 5 (Fig. 6) and underestimate the flux at the highest discharge, 2 l/s, where we
469 also see a simplification of channel morphology (Fig. 6, 3). Because we did not have tracers in the flumes we can not
470 say if the path length distributions were in fact different between the lowest and highest discharges. Future applications
471 of this method with tracer data both in the flumes and in the field could help to understand when the characteristic
472 length scale of morphology extracted by the method is an appropriate estimate of sediment transport and if this
473 corresponds to flow metrics and path length distributions. In the flume studies we tested the idea that the majority of
474 particles are bypassing the first depositional site simply by doubling the estimated path length. Assuming that sediment
475 is not trapped in the first depositional area but in the second one and doubling the path length we more closely estimate
476 the sediment transport at the higher discharges (i.e., estimates are not significantly different than the measured averages
477 ($p>0.05$) but overestimate the sediment transport at the 0.7 l/s and 1 l/s discharges ($p<0.05$) (Fig. A5).

478 **5.1.2 Confinement**

479 It is possible that due to the confined condition of the flumes, channel width may exert an outsized effect on the average
480 bedload transport distance as the channel is unable to widen in response to an increase in discharge, therefore causing a
481 flushing effect. In the flume experiment, we found that the VMD-HD method performed better at the lower discharges
482 of 0.7 l/s and 1 l/s but significantly underestimated the sediment transport at the 1.5 l/s and 2 l/s discharges (Fig. 6). The
483 underestimation at higher discharges could be related to the amount of morphological change relative to the sediment
484 transport. Recently, Booker and Eaton (2022) quantitatively explored the link between sediment transport and
485 morphology and proposed an index to represent the intuitive notion that as sediment transport increases relative to
486 morphological change, the processes become decoupled and inferences from one to another become more difficult.
487 They developed a ‘throughput index’ which is the ratio between sediment flux and morphological change and
488 represents how much sediment moves through a reach without leaving a topographic signature of equal magnitude.
489 Therefore, the ratio represents how well the flux is represented morphologically with the ratio approaching 1 when all
490 of the flux is shown as morphological change and exceeding 1 when there is transport without equivalent morphological
491 change. In our case the flume experiments were confined, therefore, as discharge increased the channel was not able to
492 widen and deform laterally potentially causing the sediment to move through the flume without leaving an equivalent
493 topographic signature. To explore the applicability of the method proposed we calculated the morphological active
494 width by counting the percentage of pixels in the DoD that showed topographic change after filtering (we applied this
495 metric only for the flume experiments since the San Juan River DoDs do not include the submerged part of the
496 channel). The morphological active width increased with discharge as expected and was positively correlated with the
497 error of our estimates (Fig. 8). This result exposes a limitation of the morphological method in general and our
498 application specifically, that is, confined channels with high transport relative to morphological change are likely poor
499 candidates for the morphological method as inferences between changes in morphology and sediment transport become
500 decoupled. Further applications of this method in the field and in the lab could identify a potential threshold defined by
501 the throughput index (Booker and Eaton, 2022) or the morphological active width described in this study. The
502 advantage of using the morphological active width as opposed to the throughput index is that it can be determined from
503 the DoD without direct sediment transport measurements.



504

505 **Figure 8: Relative percent error between estimated flux using the VMD-HD method and the measured flux in the**
 506 **flume experiments (y-axis) vs the percentage of the DoD showing morphological change (x-axis). Different**
 507 **discharges are denoted by shape.**

508 5.1.3 Morphological controls

509 Previous studies have shown that in gravel bed rivers, macroform spacing is typically 5-7 channel widths (Montgomery
 510 and Buffington, 1997) and therefore half of that spacing, i.e. pool to bar, may be considered a proxy for the
 511 characteristic path length. We compared our estimates of path length to (half) of both 5 and 7 times the channel width in
 512 the flumes and found that the IMF 5 estimates of path length were between the 5 and 7 channel widths for all but the
 513 highest discharge (Fig. A6). Interestingly, the manually measured distances were less than the 5-7 channel widths for all
 514 discharges but approaching 5 channel widths at the 2 l/s discharge (Fig. A6). When used to calculate sediment flux, the
 515 estimates derived from using 5 and 7 channel widths were not significantly different than our VMD-HD estimates at
 516 discharges 0.7-1.5 l/s or the measured flux at all discharges (Fig. A5). Here we are likely seeing a good correspondence
 517 between the characteristic path length, width, and sediment transport, because at formative discharges, morphology is
 518 the primary control on bedload travel distance. Whereas at lower discharges, where the morphology is relatively stable,
 519 discharge may exert a stronger control on path length. Because we do not have tracer data in the flumes for comparison,
 520 we can only rely on the sediment transport measurements for validation but further flume studies with both sediment
 521 flux and tracer data for validation could help resolve this question. The periodicity we extract from the DoDs as an

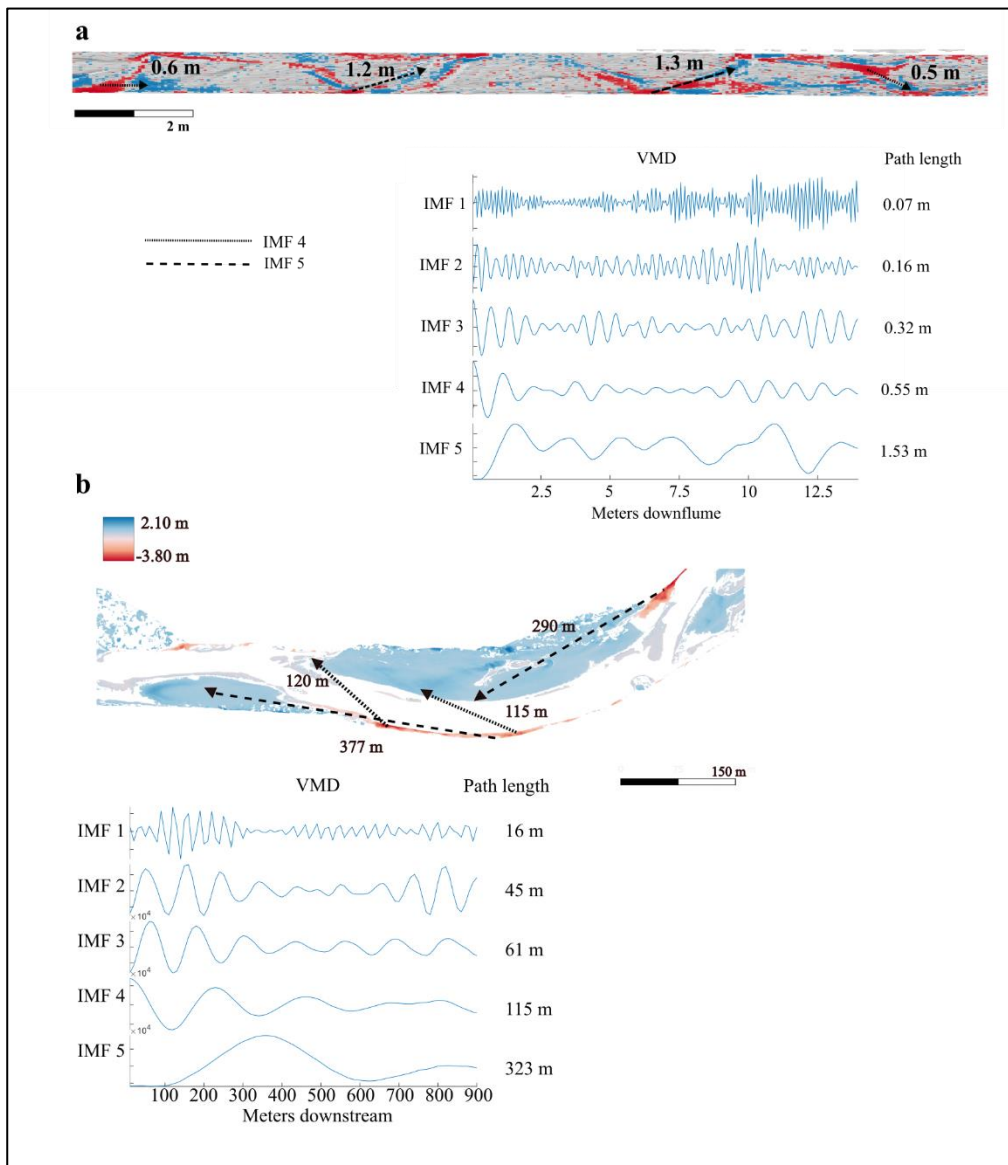
522 estimate of path length corresponds to previous observations of preferential particle deposition at specific
523 morphological units and relationships to channel morphology (Beechie, 2001; Pyrcce and Ashmore, 2003a, b; Kasprak et
524 al., 2015; McDowell and Hassan, 2020; McDowell et al., 2021). In the San Juan River study, our estimates aligned
525 closely with the secondary modes in the particle path length distributions (Fig. 7) consistent with observations that at
526 channel forming flows, particle path lengths tend to be bi or multimodal with secondary modes corresponding to the
527 location of bars (Pyrcce and Ashmore, 2003b). This preliminary result should be further examined with additional field
528 data in multi-threaded channel types.

529 We expected that the path length in more complex channels such as braided configurations would be more difficult to
530 estimate due to the possibility of multiple path lengths active at different flow stages. In this study both the flume
531 experiment and the field study exhibited a wandering morphology although in the flume experiment, the channel began
532 to simplify at higher discharges, likely due to the inability of the channel to widen in response to the increase in
533 discharge. Further, path length estimates did not change significantly between the discharges whereas the erosion
534 volume increases with discharge, and that, as mentioned previously, potentially contributed to the underestimation of
535 sediment flux at the higher discharges. Additionally, at the 1.5 l/s, and 2 l/s discharges, the patches of erosion and
536 deposition began to overlap, therefore, the wavelike pattern from areas of erosion to deposition represented by the IMF
537 5 vector became flattened (Fig. 3, A1). To disentangle the confounding erosion and deposition from the net vector, we
538 applied the VMD method to a vector created from erosion and deposition separately. When calculating the path length
539 using the erosion or deposition vectors, we took half of the resulting path length as we are still interested in the distance
540 from erosion to deposition rather than erosion to erosion. We found that the path lengths generated from these vectors
541 were not significantly different than the path lengths generated using the net vector ($p > 0.05$) (Fig. A6) nor were the
542 estimates of sediment transport (Fig. A5) This evidence supports the use of the net vector in this case because it appears
543 that erosion and deposition were similarly distributed. However, in rivers with differing morphology, perhaps braided
544 systems, we might suspect that erosion will be more localized than deposition which can be dispersed (Goff and
545 Ashmore, 1994). In these cases, using VMD to decompose the net, erosion, and deposition separately could give further
546 insight into how deposition and erosion are contributing to the net change. For example, deposition may contribute little
547 to net vector if the relative magnitude of the oscillations is small compared to erosion which tends to be more
548 concentrated. In addition to estimating a characteristic path length, this decomposition could give further insight into the
549 nature of depositional and erosional processes in a reach. We also recognize that perhaps when multiple channels are
550 present and active, it may be beneficial to segregate the DoD, treating each channel as a separate system and generate
551 multiple path length estimations and avoid compensating erosion and deposition within the cross section. Further
552 investigations are needed in the lab and in the field to propose robust methodologies to assess realistic ranges of path
553 lengths from DoD for varying river patterns.

554 **5.1.4 Using the IMFs**

555 The path length-based method for calculating sediment transport necessitates that a single path length be selected and
556 this is surely an oversimplification of reality. Encouragingly, the flume experiment shows that by using the VMD-HD
557 method to select the path length, we are able to reasonably approximate sediment transport at the lower discharges (Fig.
558 6). However, when applying this method to a real case study, like that of the San Juan River, it is important to consider
559 if the results make sense given what is known about the channel and the time and magnitude of flood events between
560 surveys, potentially taking into account both IMF 4 and IMF 5 to generate a range of plausible transport or path lengths.
561 The VMD-HD method presented here selects one of the five IMFs to be used as an estimate of path length based on the

562 geometric similarity, as measured by the Hausdorff distance, of the IMF to the original data vector. However, we
 563 presume that not only does the method occasionally select an erroneous IMF (IMF 1 for example where the path length
 564 is on the order of mm) but it also reasons that in some cases more than one IMF could represent the pattern of erosion
 565 and deposition in the DoD or perhaps a range due to the heterogeneous nature of sediment transport. In the flume
 566 experiment, the VMD-HD method selected the longest wavelength, IMF 5, 74% of the time and IMF 4, 24% of the
 567 time. There were only two instances in which IMF 1 was selected and neither IMF 2 or 3 were ever selected. Likewise,
 568 IMF 5 was selected for all three bars in the San Juan River dataset. This result agrees with observations from the signal
 569 processing literature wherein the lower frequency (in our case wavelength) IMFs (4 and 5) are thought to represent the
 570 true signal whereas the higher frequency (shorter wavelength) IMFs are attributed to noise (Boudraa et al., 2005). In our
 571 case we can verify visually that IMF 5 is most likely representative of the characteristic path length by tracing the path
 572 from erosional site to depositional site within the DoD using the manual method (Fig. 9). Here we see that the longest
 573 IMF captures the spacing between erosional and depositional patches as estimated by other methods (Redolfi, 2014;
 574 Vericat et al., 2017; Calle et al., 2020). This study, as the others, supports the idea that the periodic nature of erosion
 575 and deposition can be used to estimate sediment transport and helps to clarify the conditions where this approach is
 576 valid. Moreover, this study provides an objective and repeatable method to estimate the characteristic path length.



578 **Figure 9: DoD with arrows showing possible path lengths between areas of erosion (red) to deposition (blue)**
 579 **corresponding to both IMF 4 and IMF 5. The VMD breakdown including all IMFs and the corresponding path**
 580 **lengths are shown for an experimental run from the 1.5 l discharge (a) and bar 15 from the San Juan River (b).**

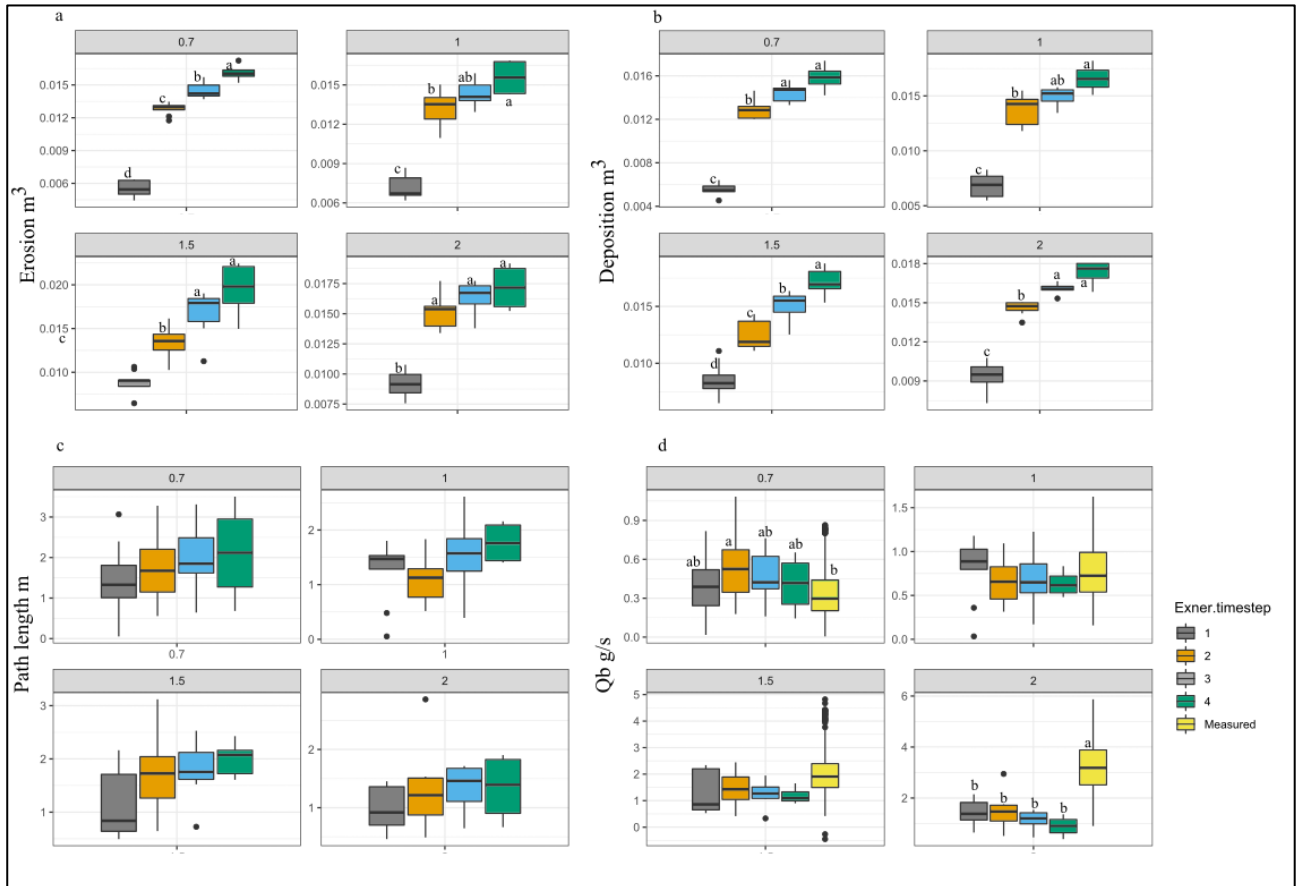
581 Different IMFs also allow us to explore multiple periodicities, such as shorter path lengths in the DoDs that may
 582 correspond to IMF 4 (Fig. 9). The method we present here to select one of the IMFs to represent the periodicity is
 583 convenient for assigning a characteristic path length to be used in sediment transport calculations. However, it is unclear
 584 if the range of IMFs may be used to estimate aspects of the path length distribution. As a first step, we see that in the
 585 San Juan River the path lengths associated with IMF 4 and IMF 5 bracket the mean, median, and key depositional areas
 586 associated with the path length distribution (Fig. 7). With future studies it may be possible to set a range of plausible
 587 transport based on IMFs 4 and 5.

588 5.2 DoD related uncertainties

589 Any application of the morphological method using DoDs is sensitive to the error thresholding method used due to the
 590 way in which different thresholding techniques influence both the volumes of erosion and deposition as well as their
 591 spatial patterning (Brasington et al., 2003; Wheaton, 2008; Wheaton et al., 2010; Vericat et al., 2017). Because our
 592 method relies on the spacing between areas of erosion and deposition which is related to the size of the patches as well
 593 as which patches are detected, we considered that thresholding techniques could greatly affect the estimates of path
 594 length. We tested this hypothesis by applying the method to both the raw and filtered DoDs for the Trento flume
 595 experiment and found that while the volumes of erosion and deposition were lower after thresholding as expected
 596 ($p < 0.001$), the path length estimates were not significantly different ($p > 0.05$) (Table A1). While the thresholding here
 597 did not affect the path length estimates, we might imagine a scenario in which an entire area of erosion or deposition is
 598 removed through aggressive thresholding techniques, thereby potentially affecting the path length estimates and
 599 therefore caution that appropriate thresholding is important for the application of this method and the morphological
 600 method in general. It is also important to consider the spatial resolution (i.e. raster cell size) of the DoD when applying
 601 this method. Similarly to thresholding or selecting a bin size, the spatial resolution of the DoD could cause information
 602 to be lost if the cell size is large enough to aggregate erosion and deposition within the same cell (see for instance the
 603 comparison made in Antoniazza et al., 2019). We see less of a risk in using smaller cell sizes as the method already
 604 calls for aggregation in the binning process and in theory VMD should be able to separate the small scale fluctuations as
 605 short wavelength IMFs. However, this is an open question and should be evaluated by the user on a case by case basis.

606 The time between surveys is of equal importance to the path length in the estimation of virtual velocity and in the field
 607 can be highly uncertain due to poor availability of hydrologic data and/or the uncertainty of estimating the onset of
 608 transport based on a critical shear stress. Further, as time between surveys increases, so too does the probability of
 609 compensating erosion and deposition which can affect both the volumes of erosion and deposition and the topographic
 610 signatures (Lindsay and Ashmore, 2002; Vericat et al., 2017) necessary for VMD-HD method. We tested how the time
 611 between surveys might affect both the volumes of erosion and deposition and our path length estimates by differencing
 612 DEMs not every time step but between two, three, and four timesteps, each time step being one of the nine runs in the
 613 lab of phase 3 (see method). Not surprisingly the volume of erosion and deposition increased significantly with
 614 increasing time between surveys with the largest increase between the 1st timestep and 2nd timestep (Fig. 10). The path
 615 length estimates did not increase significantly for any of the discharges (Fig. 10c) indicating that the path length
 616 estimate is stable, likely because, as already noted, the spacing of erosion and deposition is related to the position of
 617 erosional and depositional features which do not change much in the flume. When both of these parameters are used in
 618 the sediment transport calculations and normalized by the increased time between surveys, we found no statistically

619 significant difference between the estimates (Fig. 10d). However, though not statistically significant, there is an
 620 apparent decreasing trend in the sediment flux with the increased time between surveys, especially for the 2 l/s
 621 discharge that may indicate compensation (Fig. 10d). Despite the apparent trend at the highest discharge this is a
 622 promising result in that even by increasing the time interval by a factor of 4 we are still able to estimate sediment
 623 transport reasonably at the lower discharges. In the field there are often multiple flood events of differing magnitude in
 624 the year between surveys as was the case with the San Juan River study (McQueen et al., 2021). Although there were
 625 five flood events of differing magnitudes between the San Juan River surveys, we were still able to estimate path
 626 lengths corresponding to potentially significant features of the path length distributions (Fig. 7).



627

628 **Figure 10: (a) Erosion measured from the flume experiments for each discharge and each timestep (b) deposition**
 629 **(c) path length estimates using VMD-HD method (d) sediment flux estimated using VMD-HD method and**
 630 **measured. Significant post-hoc Tukey results are denoted by letters a-d ($\alpha=0.05$).**

631 6 Conclusion

632 Given the observed connections between morphology and path length at channel forming flows, we proposed that the
 633 periodic nature of the pattern of erosion and deposition can be a proxy for a characteristic path length in gravel bed
 634 rivers. We applied tools from signal processing to quantify this periodicity and found that by the longest wavelengths
 635 from the decomposition, IMF 4 and IMF 5 may represent meaningful bedload transport processes and IMF 5 in
 636 particular may represent the characteristic path length. We found that the path length estimates generated by IMFs 4 and
 637 5 bracket a significant portion of measured path length distributions in the field and correspond to important
 638 morphological units. In the flume experiment we found that IMF 4 and 5 path lengths also bracket the manually
 639 measured distances between erosional and depositional patches and when extended to calculate sediment flux our
 640 estimates were not significantly different from the measured average at low discharges. Importantly we found an

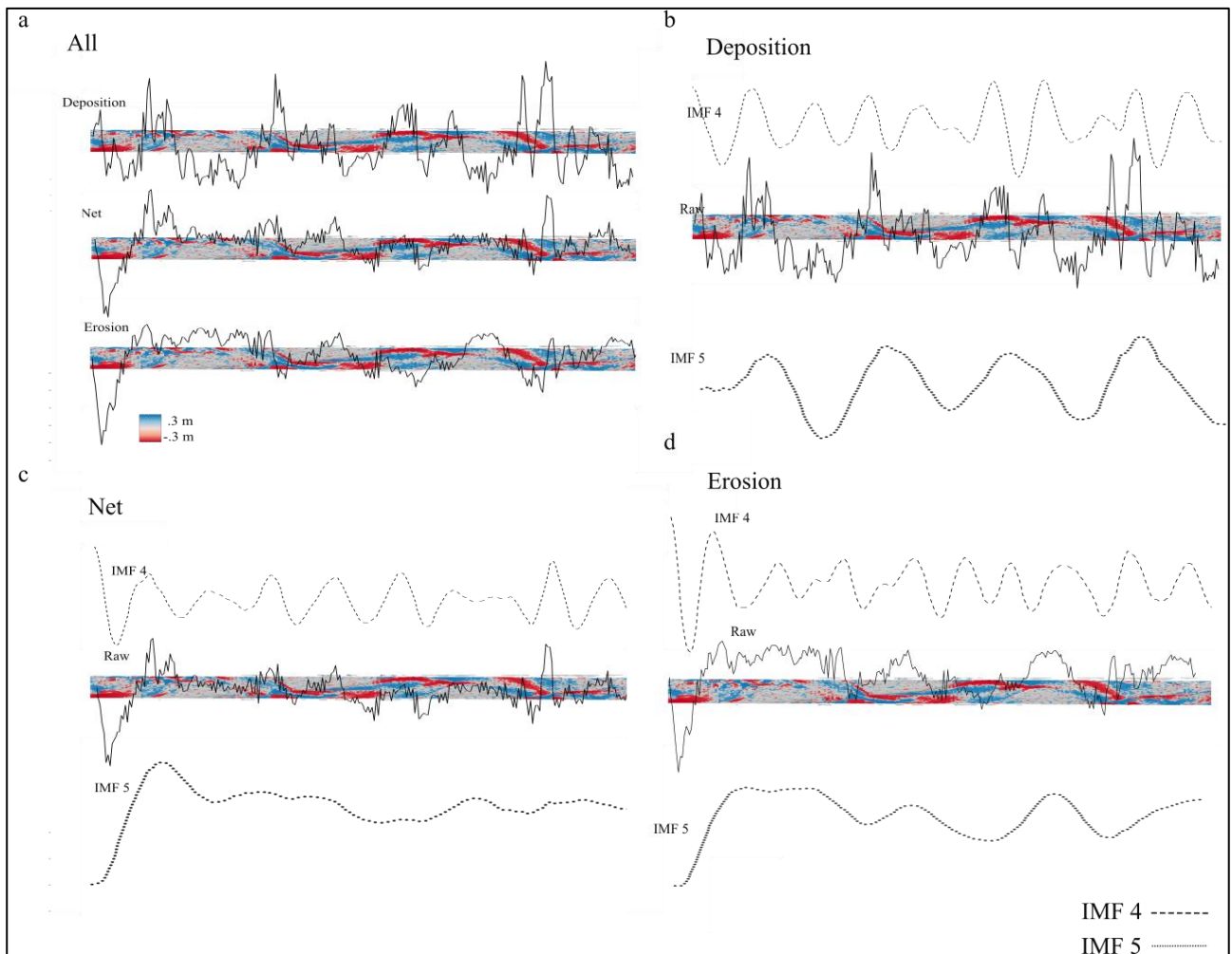
641 insensitivity of the method to increasing discharge and propose that perhaps limits arise where discharge increases in
 642 confined settings, such as in the flume, and sediment transport becomes decoupled from morphological changes. Our
 643 method provides a new view of the periodic nature of erosion and deposition in sediment transport and a novel way to
 644 extract sediment transport information using only DoDs.

645

646

647 Appendix A

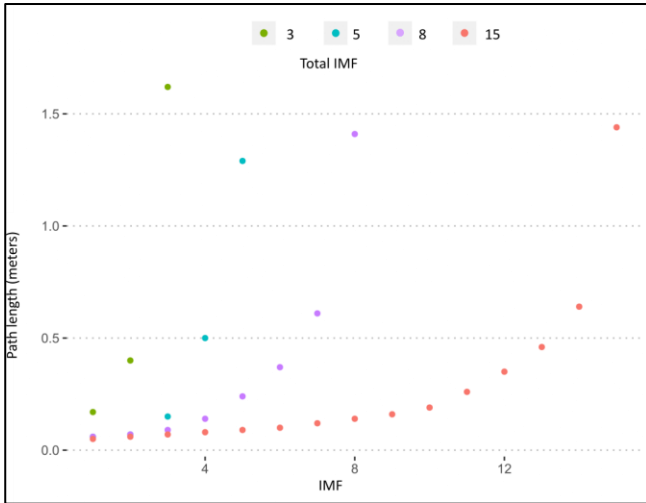
648



649

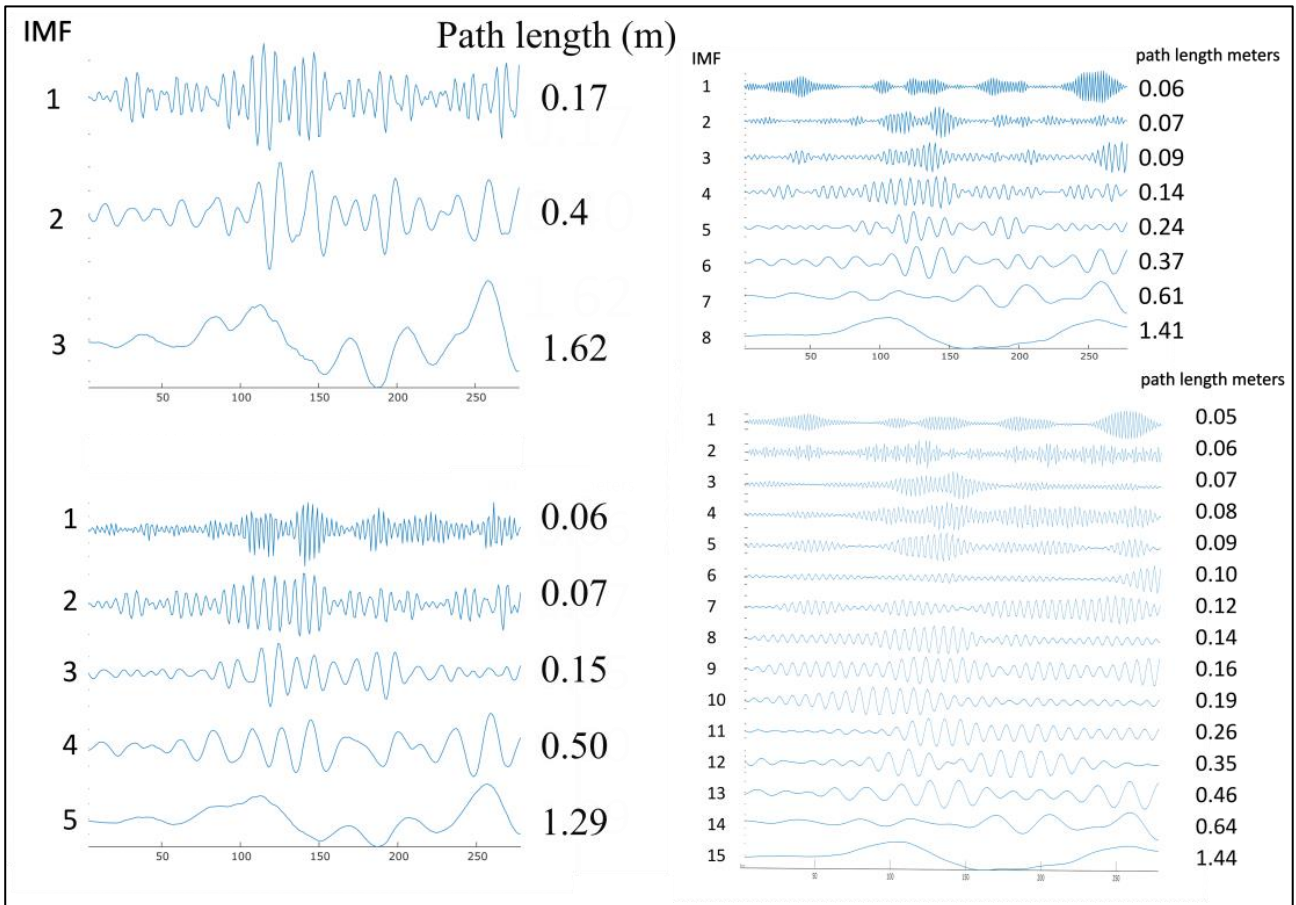
650 Figure A1. DoDs from the 2 l/s discharge. a) Vector of deposition, erosion, and the net. b) Raw depositional vector and
 651 the decomposition of IMF 4 and IMF 5 from that depositional vector. c) Net vector and the decomposition of IMF 4 and
 652 IMF 5 from that net vector. d) Raw erosional vector and the decomposition of IMF 4 and IMF 5 from that erosional
 653 vector.

654



655

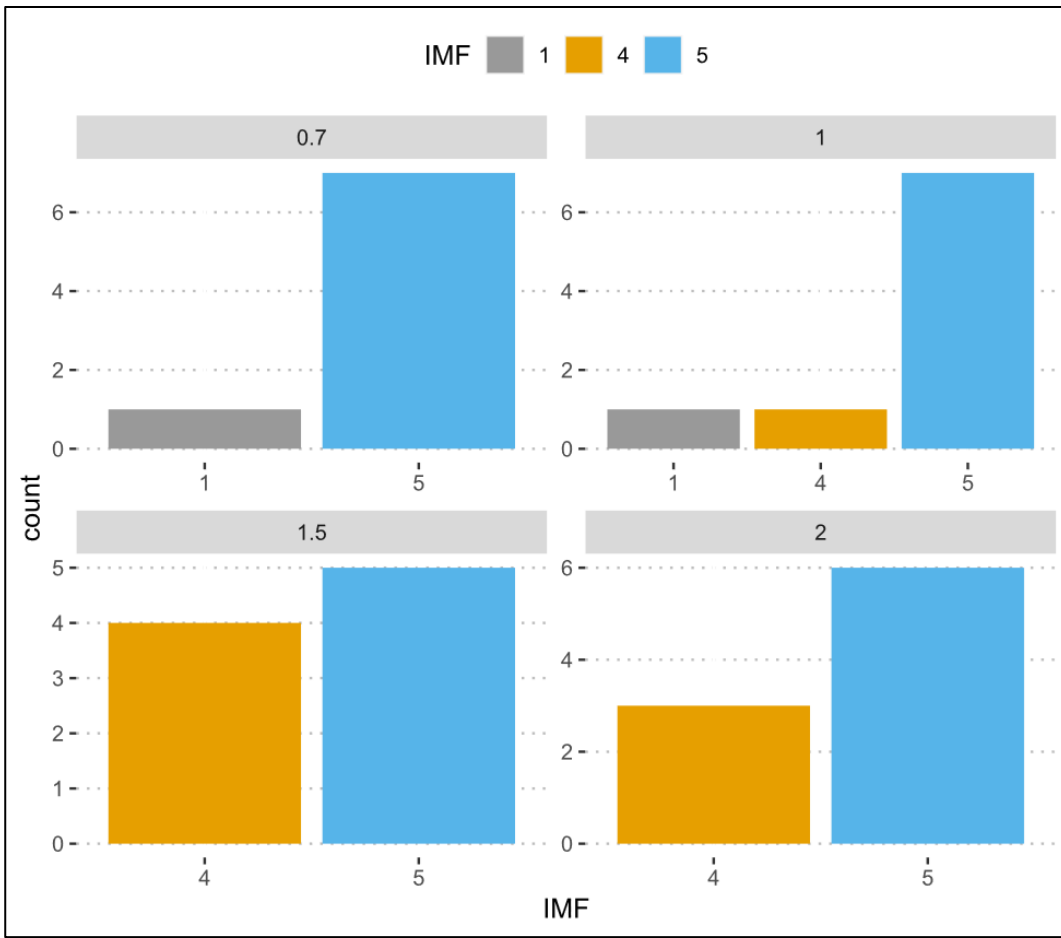
656 Figure A2. Path length estimates using a maximum of 3,5,8, or 15 IMFs.



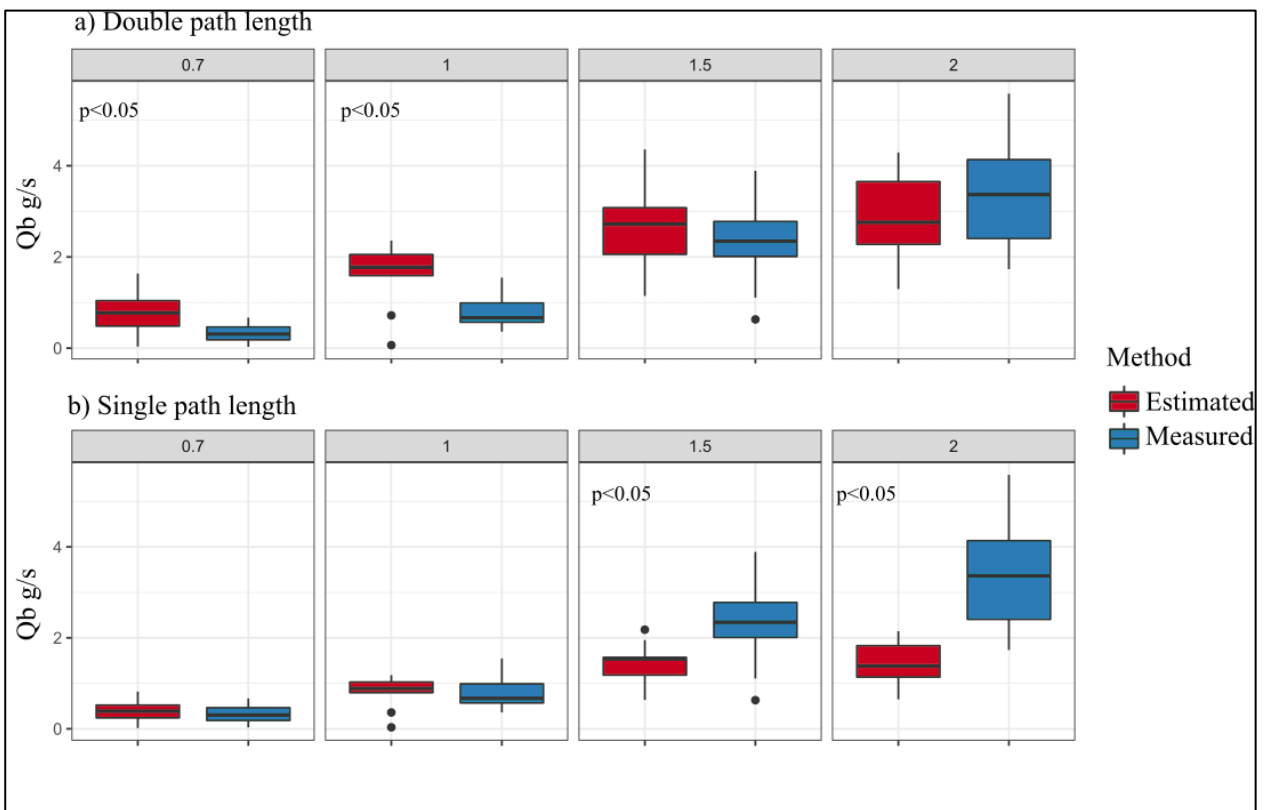
657

658 Figure A3. Path length estimates from VMD for 1.5 l/s discharge. Sensitivity of maximum number of IMFs.

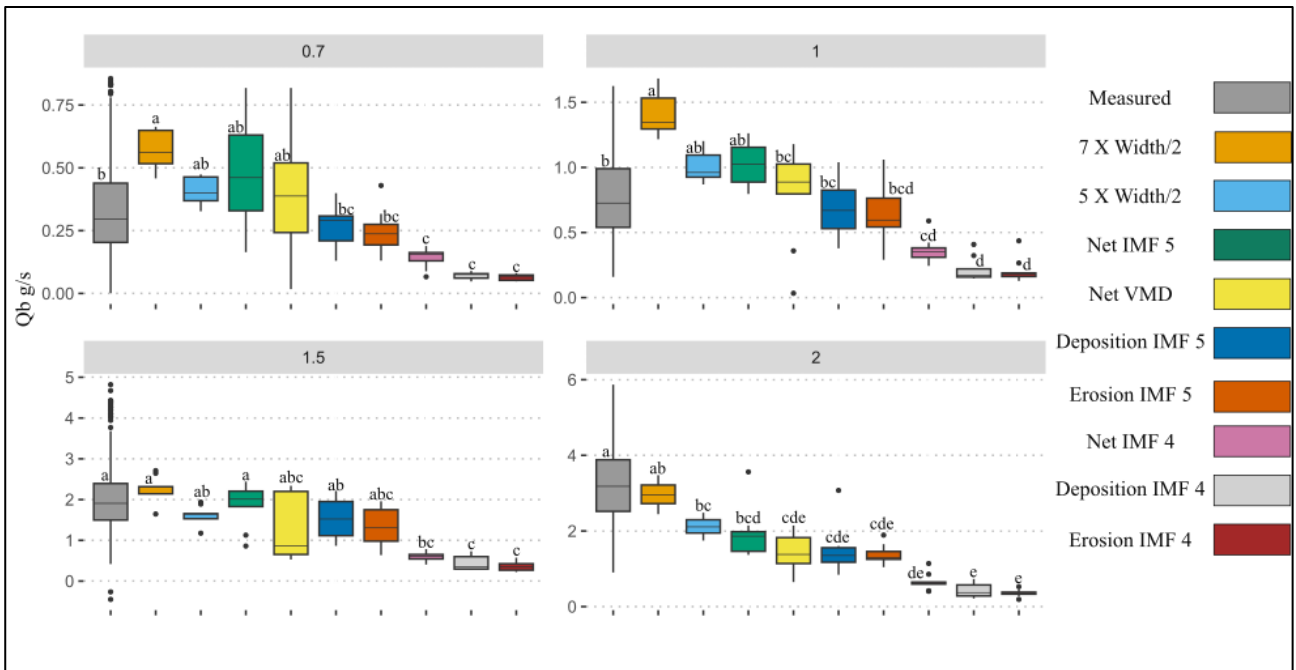
659



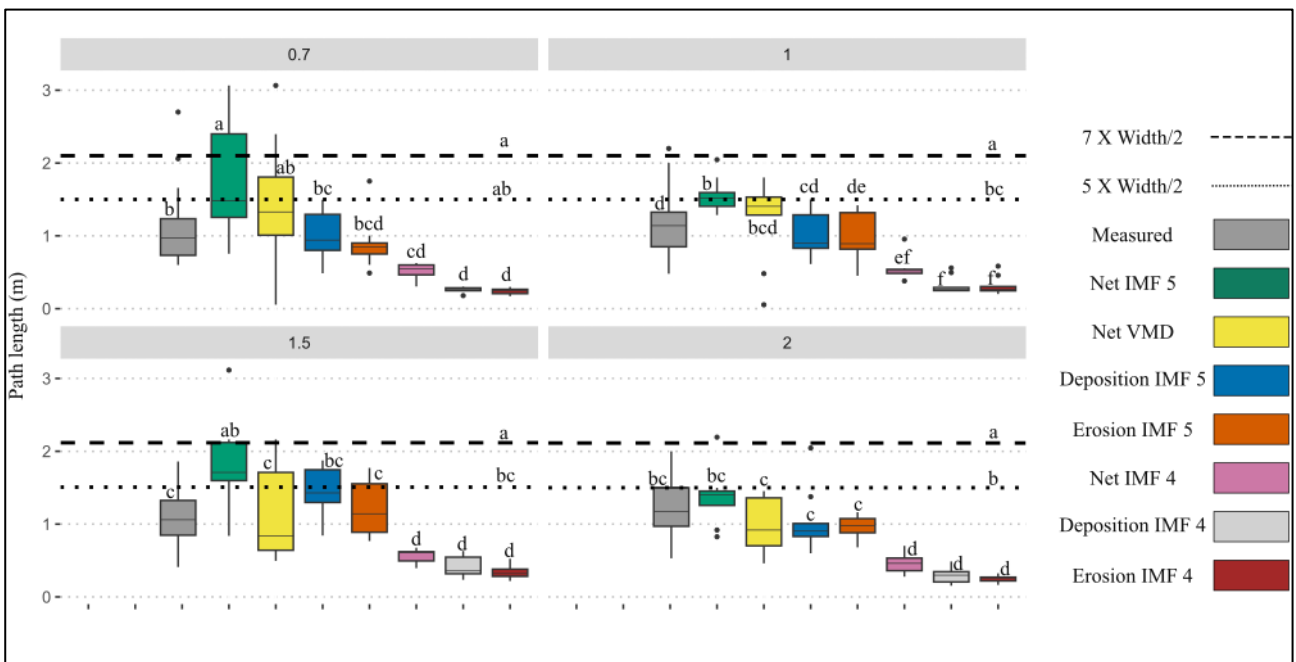
660
661 Figure A4. Number of times each IMF was selected by the VMD-HD method for each discharge.



663 Figure A5. Sediment transport calculated using the single path length estimate from the VMD-HD method (b) and
 664 doubling the path length estimate (a). Estimated flux is red and measured flux is blue. Significant p values are shown.
 665



666
 667 Figure A6. Sediment transport (g/s) calculated using channel dimensions, IMFs 4 and 5 for net, erosion, and deposition
 668 vectors. Compared to the measured flux for each discharge. Post hoc Tukey results denoted by letters a-f.



669
 670 Figure A7. Path length estimates from the channel dimensions, IMFs 4 and 5 for net, erosion, and deposition
 671 vectors compared to manually measured distances for each discharge. Post hoc Tukey results denoted by letters a-f.

672 Table A1. Results from filtered vs raw DoDs from the flume experiments.

Discharge	Path length raw (m)	Path length filtered (m)	Qb estimated raw(g/s)	Qb estimated filtered (g/s)	Erosion raw (m3)	Deposition raw(m3)	Erosion filtered (m3)	Deposition filtered (m3)
-----------	---------------------	--------------------------	-----------------------	-----------------------------	------------------	--------------------	-----------------------	--------------------------

0.7	1.77	1.31	0.69	0.30	0.01	0.01	0.01	0.01
0.7	0.80	0.75	0.29	0.14	0.01	0.01	0.00	0.00
0.7	3.05	3.06	1.20	0.71	0.01	0.01	0.01	0.01
0.7	2.54	2.40	0.97	0.51	0.01	0.01	0.01	0.01
0.7	2.30	0.05	1.01	0.01	0.01	0.01	0.01	0.01
0.7	0.87	1.09	0.35	0.23	0.01	0.01	0.01	0.01
0.7	1.57	1.61	0.70	0.43	0.01	0.01	0.01	0.01
0.7	1.24	1.35	0.56	0.37	0.01	0.01	0.01	0.01
1	1.25	1.41	1.04	0.89	0.01	0.01	0.01	0.01
1	1.37	0.48	1.28	0.31	0.01	0.01	0.01	0.01
1	1.25	1.47	1.10	1.02	0.01	0.01	0.01	0.01
1	1.23	1.80	1.18	1.00	0.01	0.01	0.01	0.01
1	1.48	1.59	1.46	0.84	0.01	0.01	0.01	0.01
1	1.83	1.53	1.57	0.77	0.01	0.01	0.01	0.01
1	1.54	1.52	1.27	0.75	0.01	0.01	0.01	0.01
1	1.51	1.29	1.21	0.69	0.01	0.01	0.01	0.01
1.5	1.12	0.68	1.82	0.53	0.01	0.01	0.01	0.01
1.5	1.63	0.84	2.30	0.86	0.01	0.01	0.01	0.01
1.5	1.50	0.64	2.74	0.65	0.02	0.01	0.01	0.01
1.5	0.50	0.61	0.82	0.67	0.01	0.01	0.01	0.01
1.5	0.85	0.49	1.41	0.54	0.01	0.01	0.01	0.01
1.5	0.51	1.60	0.76	2.01	0.01	0.01	0.01	0.01
1.5	1.67	1.71	2.28	2.21	0.01	0.01	0.01	0.01
1.5	1.50	2.16	2.54	2.20	0.01	0.01	0.01	0.01
1.5	1.13	2.12	1.73	2.34	0.01	0.01	0.01	0.01
2	1.41	1.40	2.53	1.86	0.01	0.01	0.01	0.01
2	0.91	0.92	1.58	1.19	0.01	0.01	0.01	0.01
2	1.26	1.36	2.05	1.58	0.01	0.01	0.01	0.01
2	1.13	1.26	1.67	1.27	0.01	0.01	0.01	0.01
2	0.06	1.45	0.09	1.61	0.01	0.01	0.01	0.01
2	0.46	0.46	0.78	0.56	0.01	0.01	0.01	0.01
2	1.32	0.83	2.04	1.18	0.01	0.01	0.01	0.01
2	0.71	0.66	1.30	0.74	0.01	0.01	0.01	0.01
Summary								
Discharge	Erosion	Deposition	Path Length	Qb				
0.7	p<0.001**	p<0.001**	p>0.05	p<0.05*				
1	p<0.001**	p<0.001**	p>0.05	p<0.05*				
1.5	p<0.001**	p<0.001**	p>0.05	p<0.05*				
2	p<0.001**	p<0.001**	p>0.05	p>0.05				
*p-values from student's t test between raw and filtered data								

673

674 **Data availability**675 Data is available at <https://doi.org/10.5281/zenodo.8014453>.

676 **Author contribution**

677 LC, SB, WB and NS conceptualized the study. EP preformed the experiments. LC, SB and WB designed the method.
678 LC performed statistical analysis. LC, EP, and WB wrote the manuscript. LC, SB, EP, WB, and NS edited the
679 manuscript.

680 **Competing interests**

681 The authors declare they have no competing interests.

682 **Financial support**

683 This work was supported by the CARIPARO foundation and the University of Padova.

684 **References**

- 685 Antoniazza, G., Bakker, M., and Lane, S. N.: Revisiting the morphological method in two-dimensions to quantify bed-
686 material transport in braided rivers, *Earth Surf. Process. Landf.*, 44, 2251–2267, <https://doi.org/10.1002/esp.4633>, 2019.
- 687 Ashmore, P. E. and Church, M.: Sediment transport and river morphology: a paradigm for study, *Gravel-Bed Rivers*
688 *Environ.*, 345, 115–139, 1998.
- 689 Bakker, M., Antoniazza, G., Odermatt, E., and Lane, S. N.: Morphological Response of an Alpine Braided Reach to
690 Sediment-Laden Flow Events, *J. Geophys. Res. Earth Surf.*, 124, 1310–1328, <https://doi.org/10.1029/2018JF004811>,
691 2019.
- 692 Barnhart, B. L. and Eichinger, W. E.: Empirical Mode Decomposition applied to solar irradiance, global temperature,
693 sunspot number, and CO2 concentration data, *J. Atmospheric Sol.-Terr. Phys.*, 73, 1771–1779,
694 <https://doi.org/10.1016/j.jastp.2011.04.012>, 2011.
- 695 Beechie, T. J.: Empirical predictors of annual bed load travel distance, and implications for salmonid habitat restoration
696 and protection, *Earth Surf. Process. Landf.*, 26, 1025–1034, <https://doi.org/10.1002/esp.251>, 2001.
- 697 Booker, W. H. and Eaton, B. C.: Morphodynamic styles: characterising the behaviour of gravel-bed rivers using a
698 novel, quantitative index, *Earth Surf. Dyn.*, 10, 247–260, <https://doi.org/10.5194/esurf-10-247-2022>, 2022.
- 699 Boudraa, A.-O., Cexus, J.-C., and Saidi, Z.: EMD-Based Signal Noise Reduction, *Signal Process.*, 1, 2005.
- 700 Brasington, J., Rumsby, B. T., and McVey, R. A.: Monitoring and modelling morphological change in a braided gravel-
701 bed river using high resolution GPS-based survey, *Earth Surf. Process. Landf.*, 25, 973–990,
702 [https://doi.org/10.1002/1096-9837\(200008\)25:9<973::AID-ESP111>3.0.CO;2-Y](https://doi.org/10.1002/1096-9837(200008)25:9<973::AID-ESP111>3.0.CO;2-Y), 2000.
- 703 Brasington, J., Langham, J., and Rumsby, B.: Methodological sensitivity of morphometric estimates of coarse fluvial
704 sediment transport, *Geomorphology*, 53, 299–316, [https://doi.org/10.1016/S0169-555X\(02\)00320-3](https://doi.org/10.1016/S0169-555X(02)00320-3), 2003.
- 705 Brenna, A. and Surian, N.: Coarse sediment mobility and fluxes in wide mountain streams: Insights using the virtual
706 velocity approach, *Geomorphology*, 427, 108625, <https://doi.org/10.1016/j.geomorph.2023.108625>, 2023.
- 707 Brenna, A., Surian, N., and Mao, L.: Virtual Velocity Approach for Estimating Bed Material Transport in Gravel-Bed
708 Rivers: Key Factors and Significance, *Water Resour. Res.*, 55, 1651–1674, <https://doi.org/10.1029/2018WR023556>,
709 2019.
- 710 Brenna, A., Surian, N., Ghinassi, M., and Marchi, L.: Sediment–water flows in mountain streams: Recognition and
711 classification based on field evidence, *Geomorphology*, 371, 107413, <https://doi.org/10.1016/j.geomorph.2020.107413>,
712 2020.
- 713 Brewer, P. A. and Passmore, D. G.: Sediment budgeting techniques in gravel-bed rivers, *Geol. Soc. Lond. Spec. Publ.*,
714 191, 97–113, <https://doi.org/10.1144/GSL.SP.2002.191.01.07>, 2002.
- 715 Calle, M., Calle, J., Alho, P., and Benito, G.: Inferring sediment transfers and functional connectivity of rivers from
716 repeat topographic surveys, *Earth Surf. Process. Landf.*, 45, 681–693, <https://doi.org/10.1002/esp.4765>, 2020.
- 717 Church, M.: Bed Material Transport and the Morphology of Alluvial River Channels, *Annu. Rev. Earth Planet. Sci.*, 34,
718 325–354, <https://doi.org/10.1146/annurev.earth.33.092203.122721>, 2006.

- 719 Dragomiretskiy, K. and Zosso, D.: Variational Mode Decomposition, *IEEE Trans. Signal Process.*, 62, 531–544,
720 <https://doi.org/10.1109/TSP.2013.2288675>, 2014.
- 721 Ferguson, R. I. and Ashworth, P. J.: Spatial patterns of bedload transport and channel change in braided and near-
722 braided rivers, *Dyn. Gravel-Bed Rivers Billi P Hey RD Thorne CR Tacconi P Eds*, 1992.
- 723 Garcia Lugo, G. A., Bertoldi, W., Henshaw, A. J., and Gurnell, A. M.: The effect of lateral confinement on gravel bed
724 river morphology, *Water Resour. Res.*, 51, 7145–7158, <https://doi.org/10.1002/2015WR017081>, 2015.
- 725 Goff, J. R. and Ashmore, P.: Gravel transport and morphological change in braided sunwapta river, Alberta, Canada,
726 *Earth Surf. Process. Landf.*, 19, 195–212, <https://doi.org/10.1002/esp.3290190302>, 1994.
- 727 Grams, P. E., Topping, D. J., Schmidt, J. C., Hazel Jr., J. E., and Kaplinski, M.: Linking morphodynamic response with
728 sediment mass balance on the Colorado River in Marble Canyon: Issues of scale, geomorphic setting, and sampling
729 design, *J. Geophys. Res. Earth Surf.*, 118, 361–381, <https://doi.org/10.1002/jgrf.20050>, 2013.
- 730 Grams, P. E., Buscombe, D., Topping, D. J., Kaplinski, M., and Hazel, J. E.: How many measurements are required to
731 construct an accurate sand budget in a large river? Insights from analyses of signal and noise, *Earth Surf. Process.*
732 *Landf.*, 44, 160–178, <https://doi.org/10.1002/esp.4489>, 2019.
- 733 Hassan, M. A. and Bradley, D. N.: Geomorphic Controls on Tracer Particle Dispersion in Gravel-Bed Rivers, in:
734 *Gravel-Bed Rivers*, John Wiley & Sons, Ltd, 159–184, <https://doi.org/10.1002/9781118971437.ch6>, 2017.
- 735 Hassan, M. A., Church, M., and Schick, A. P.: Distance of movement of coarse particles in gravel bed streams, *Water*
736 *Resour. Res.*, 27, 503–511, <https://doi.org/10.1029/90WR02762>, 1991.
- 737 Hassan, M. A., Church, M., and Ashworth, P. J.: Virtual rate and mean distance of travel of individual clasts in gravel-
738 bed channels, *Earth Surf. Process. Landf.*, 17, 617–627, <https://doi.org/10.1002/esp.3290170607>, 1992.
- 739 Huang, N., Chen, H., Cai, G., Fang, L., and Wang, Y.: Mechanical Fault Diagnosis of High Voltage Circuit Breakers
740 Based on Variational Mode Decomposition and Multi-Layer Classifier, *Sensors*, 16, 1887,
741 <https://doi.org/10.3390/s16111887>, 2016.
- 742 Kasprak, A., Wheaton, J. M., Ashmore, P. E., Hensleigh, J. W., and Peirce, S.: The relationship between particle travel
743 distance and channel morphology: results from physical models of braided rivers., *J. Geophys. Res. Earth Surf.*, 120,
744 55–74, 2015.
- 745 Lane, S. N., Richards, K. S., and Chandler, J. H.: Morphological Estimation of the Time-Integrated Bed Load Transport
746 Rate, *Water Resour. Res.*, 31, 761–772, <https://doi.org/10.1029/94WR01726>, 1995.
- 747 Lane, S. N., Westaway, R. M., and Murray Hicks, D.: Estimation of erosion and deposition volumes in a large, gravel-
748 bed, braided river using synoptic remote sensing, *Earth Surf. Process. Landf.*, 28, 249–271,
749 <https://doi.org/10.1002/esp.483>, 2003.
- 750 Liébault, F., Bellot, H., Chapuis, M., Klotz, S., and Deschâtres, M.: Bedload tracing in a high-sediment-load mountain
751 stream: Bedload tracing in a high-sediment-load mountain stream, *Earth Surf. Process. Landf.*, 37, 385–399,
752 <https://doi.org/10.1002/esp.2245>, 2012.
- 753 Lindsay, J. B. and Ashmore, P. E.: The effects of survey frequency on estimates of scour and fill in a braided river
754 model, *Earth Surf. Process. Landf.*, 27, 27–43, <https://doi.org/10.1002/esp.282>, 2002.
- 755 Liu, S., He, Q., Gao, R. X., and Freedson, P.: Empirical mode decomposition applied to tissue artifact removal from
756 respiratory signal, in: 2008 30th Annual International Conference of the IEEE Engineering in Medicine and Biology
757 Society, 2008 30th Annual International Conference of the IEEE Engineering in Medicine and Biology Society, 3624–
758 3627, <https://doi.org/10.1109/IEMBS.2008.4649991>, 2008.
- 759 Ma, W., Yin, S., Jiang, C., and Zhang, Y.: Variational mode decomposition denoising combined with the Hausdorff
760 distance, *Rev. Sci. Instrum.*, 88, 035109, <https://doi.org/10.1063/1.4978029>, 2017.

- 761 Mao, L., Picco, L., Lenzi, M. A., and Surian, N.: Bed material transport estimate in large gravel-bed rivers using the
762 virtual velocity approach: Virtual velocity for bed material transport estimate, *Earth Surf. Process. Landf.*, 42, 595–611,
763 <https://doi.org/10.1002/esp.4000>, 2017.
- 764 McDowell, C. and Hassan, M. A.: The influence of channel morphology on bedload path lengths: Insights from a
765 survival process model, *Earth Surf. Process. Landf.*, 45, 2982–2997, <https://doi.org/10.1002/esp.4946>, 2020.
- 766 McDowell, C., Gaeuman, D., and Hassan, M. A.: Linkages between bedload displacements and topographic change,
767 *Earth Surf. Process. Landf.*, 46, 3127–3142, <https://doi.org/10.1002/esp.5221>, 2021.
- 768 McLean, D. G. and Church, M.: Sediment transport along lower Fraser River: 2. Estimates based on the long-term
769 gravel budget, *Water Resour. Res.*, 35, 2549–2559, <https://doi.org/10.1029/1999WR900102>, 1999.
- 770 McQueen, R., Ashmore, P., Millard, T., and Goeller, N.: Bed Particle Displacements and Morphological Development
771 in a Wandering Gravel-Bed River, *Water Resour. Res.*, 57, <https://doi.org/10.1029/2020WR027850>, 2021.
- 772 Montgomery, D. R. and Buffington, J. M.: Channel-reach morphology in mountain drainage basins, *GSA Bull.*, 109,
773 596–611, [https://doi.org/10.1130/0016-7606\(1997\)109<0596:CRMIMD>2.3.CO;2](https://doi.org/10.1130/0016-7606(1997)109<0596:CRMIMD>2.3.CO;2), 1997.
- 774 Pyrce, R. and Ashmore, P.: The relation between particle path length distributions and channel morphology in gravel-
775 bed streams: A synthesis, *Geomorphology*, 56, 167–187, [https://doi.org/10.1016/S0169-555X\(03\)00077-1](https://doi.org/10.1016/S0169-555X(03)00077-1), 2003a.
- 776 Pyrce, R. S. and Ashmore, P. E.: Particle path length distributions in meandering gravel-bed streams: results from
777 physical models, *Earth Surf. Process. Landf.*, 28, 951–966, <https://doi.org/10.1002/esp.498>, 2003b.
- 778 Pyrce, R. S. and Ashmore, P. E.: Bedload path length and point bar development in gravel-bed river models,
779 *Sedimentology*, 52, 839–857, <https://doi.org/10.1111/j.1365-3091.2005.00714.x>, 2005.
- 780 Redolfi, M.: Sediment transport and morphology of braided rivers: steady and unsteady regime, n.d.
- 781 Roux, C., Alber, A., Bertrand, M., Vaudor, L., and Piégay, H.: “FluvialCorridor”: A new ArcGIS toolbox package for
782 multiscale riverscape exploration, *Geomorphology*, 242, 29–37, <https://doi.org/10.1016/j.geomorph.2014.04.018>, 2015.
- 783 Schneider, J. M., Turowski, J. M., Rickenmann, D., Hegglin, R., Arrigo, S., Mao, L., and Kirchner, J. W.: Scaling
784 relationships between bed load volumes, transport distances, and stream power in steep mountain channels, *J. Geophys.*
785 *Res. Earth Surf.*, 119, 533–549, <https://doi.org/10.1002/2013JF002874>, 2014.
- 786 Sigmund, M.: *Voice Recognition by Computer*, Tectum Verlag DE, 114 pp., 2003.
- 787 Upadhyay, A. and Pachori, R. B.: Instantaneous voiced/non-voiced detection in speech signals based on variational
788 mode decomposition, *J. Frankl. Inst.*, 352, 2679–2707, <https://doi.org/10.1016/j.jfranklin.2015.04.001>, 2015.
- 789 Vázquez-Tarrío, D. and Batalla, R. J.: Assessing Controls on the Displacement of Tracers in Gravel-Bed Rivers, *Water*,
790 11, 1598, <https://doi.org/10.3390/w11081598>, 2019.
- 791 Vázquez-Tarrío, D., Recking, A., Liébault, F., Tal, M., and Menéndez-Duarte, R.: Particle transport in gravel-bed
792 rivers: Revisiting passive tracer data: Particle transport in gravel-bed rivers, *Earth Surf. Process. Landf.*, 44, 112–128,
793 <https://doi.org/10.1002/esp.4484>, 2019.
- 794 Vericat, D., Wheaton, J. M., and Brasington, J.: Revisiting the Morphological Approach, in: *Gravel-Bed Rivers*, John
795 Wiley & Sons, Ltd, 121–158, <https://doi.org/10.1002/9781118971437.ch5>, 2017.
- 796 Wheaton, J. M.: Uncertainty in morphological sediment budgeting of rivers, phd, University of Southampton, 2008.
- 797 Wheaton, J. M., Brasington, J., Darby, S. E., and Sear, D. A.: Accounting for uncertainty in DEMs from repeat
798 topographic surveys: improved sediment budgets, *Earth Surf. Process. Landf.*, 35, 136–156,
799 <https://doi.org/10.1002/esp.1886>, 2010.
- 800 Wilcock, P. R.: Entrainment, displacement and transport of tracer gravels, *Earth Surf. Process. Landf.*, 22, 1125–1138,
801 [https://doi.org/10.1002/\(SICI\)1096-9837\(199712\)22:12<1125::AID-ESP811>3.0.CO;2-V](https://doi.org/10.1002/(SICI)1096-9837(199712)22:12<1125::AID-ESP811>3.0.CO;2-V), 1997.

802 Wu, S., Feng, F., Zhu, J., Wu, C., and Zhang, G.: A Method for Determining Intrinsic Mode Function Number in
803 Variational Mode Decomposition and Its Application to Bearing Vibration Signal Processing, *Shock Vib.*, 2020, 1–16,
804 <https://doi.org/10.1155/2020/8304903>, 2020.

805